International
Progress Report

IPR-01-01

Äspö Hard Rock Laboratory

Prototype Repository

Acoustic emission and ultrasonic monitoring during the excavation of deposition holes in the Prototype Repository

Dr. Will Pettitt
Dr. Calum Baker

Applied Seismology Consultants

Prof. R Paul Young

Liverpool University

December 1999

Svensk Kärnbränslehantering AB
Swedish Nuclear Fuel
and Waste Management Co
Box 5864
SE-102 40 Stockholm Sweden
Tel +46 8 459 84 00
Fax +46 8 661 57 19

Äspö Hard Rock
Laboratory

Report no.	No.
IPR-01-01	F63K
Author	Date
Dr. W Pettitt, Dr. C Baker, Prof. R P Young	99-12-25
Checked by	Date
Jörgen Söderhäll	00-08-08
Approved	Date
Christer Svemar	01-05-03

Äspö Hard Rock Laboratory

Prototype Repository

Acoustic emission and ultrasonic monitoring during the excavation of deposition holes in the Prototype Repository

Dr. Will Pettitt
Dr. Calum Baker

Applied Seismology Consultants

Prof. R Paul Young

Liverpool University

December 1999

Keywords: Acoustic emission, Prototype Repository, EDZ, ultrasonic sound

Executive Summary

Two deposition holes have been excavated as part of the Prototype Repository at the Hard Rock Laboratory, Sweden using a large diameter boring machine. The holes are 1.75m in diameter and 8.8m in length and were excavated in eleven 0.8m rounds. An ultrasonic array was installed around each deposition hole to investigate the response of the rock mass to the excavation. Acoustic emission (AE) monitoring has been used to delineate zones of stress-related fracturing around the deposition hole perimeter. Changes in ultrasonic velocities, measured every hour, have been used to investigate the response of the rock mass over a broader time and volume than the AE scale, and to quantitatively measure the accumulation of fracturing in the damaged zone.

A total of 2467 AE triggers were obtained during monitoring of the two deposition holes. Of these 1153 were located. There was significantly more AE activity around the second deposition hole (labelled DA3545G01) than the first (DA3551G01). This difference is likely to be dependent upon intersection of the excavation with a greater number of pre-existing fractures. These fractures may be preferentially located in the side wall of the deposition hole or preferentially orientated to the in situ stress field. Breakout fracturing has been observed with AEs distributed mainly in regions orthogonal to the maximum principal stress, σ_1. This is consistent with observations from the Canister Retrieval Tunnel and from dynamic numerical models. AEs, and hence microcrack damage, are shown to locate in clusters down the deposition hole and not as a continuous 'thin skin'. These clusters are probably associated with weaknesses in the rock mass generated by excavation through pre-existing fractures. AE results from the Prototype Repository and the Canister Retrieval Tunnel show that damage in the side wall of the deposition holes depends significantly on these pre-existing features. The in situ stress field is a contributing factor in that induced stresses are sufficiently high to create damage in these weakened regions although not sufficiently high to create significant damage in the rock mass as a whole. It is suggested that any follow up study relate AE clustering to mapped fractures in the deposition holes and to modelled stress regimes.

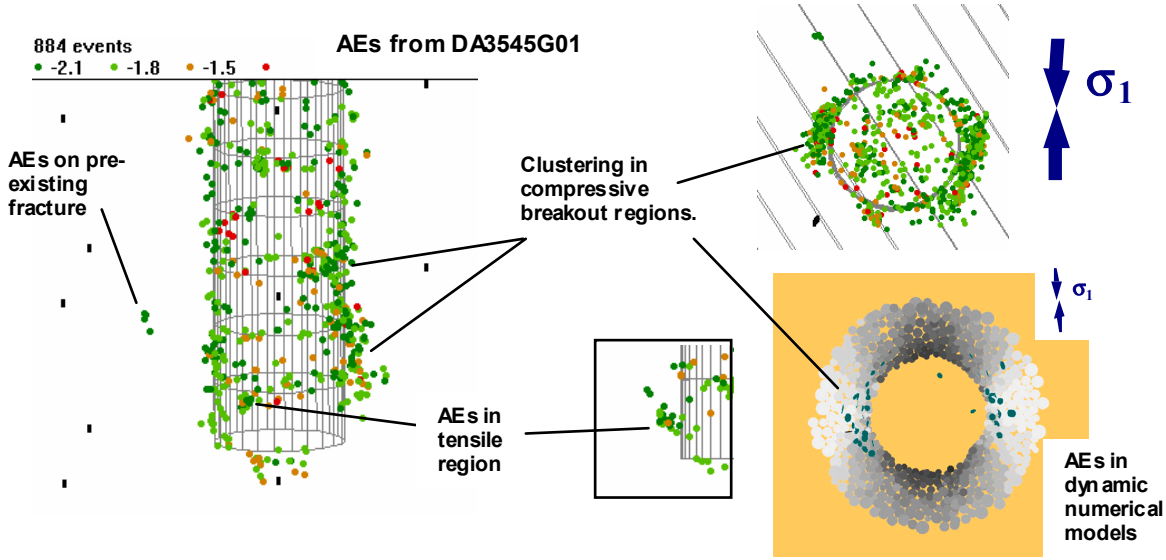

AE locations from excavation of deposition hole DD0092G01 in the Canister Retrieval Test.

The damaged zone in the breakout regions has been mapped extending 20-30cm into the side wall. The scale of fracturing, from calibration studies, is believed to be of the order of millimetres in dimension. Changes in ultrasonic velocities are shown to be approximately 10-30m.s^{-1} through regions of unloaded compressive stress - or tensile stress - in a simple Kirsch solution. These changes occur during excavation of a few rounds as the deposition hole passes the ray path. This agrees with the time dependency of AEs showing that stress-induced fracturing is most severe in the first 24 hours after excavation of a round. The mean change in velocity for 'skimming' ray paths, that pass the excavation by only a few centimetres, is approximately -15m.s^{-1}. This is an identical result to that obtained in the Retrieval Tunnel and describes a 15% reduction in dynamic Young's modulus in the excavation damaged zone. Changes in velocity are observed to be dependent on the ray path orientation relative to the deposition hole. Ray paths that pass through regions of low compressive stress describe larger changes in velocity than ray paths through regions of high compressive stress. This is due to fractures in the unloaded regions being preferentially opened.

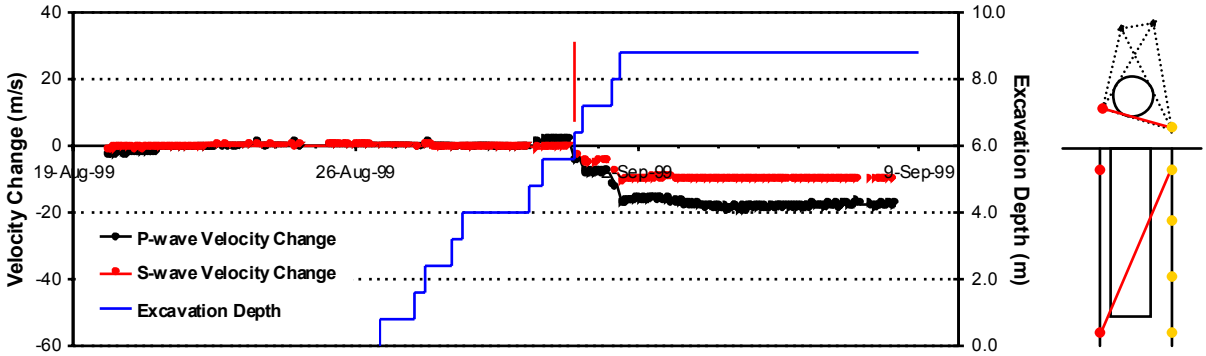

The AE distributions and velocity changes measured in the Prototype Repository are consistent with those obtained in the Canister Retrieval Tunnel and are consistent within approximately 15° azimuth of an average in situ stress tensor calculated from Leijon[1995] (σ_1 has an azimuth of 131°EofN). However, they are not consistent with the orientations of in situ stresses in the Prototype Repository (σ_1 has an azimuth of 188°EofN) measured by Ljunggren and Bergsten[1998]. It is recommended that further in situ stress measurements are conducted at the 450m level to resolve inconsistencies in the stress measurements.

A CD is included with this report presenting AE locations for the two deposition holes. The user can interactively step through the data in time and also control the view orientation and magnification.

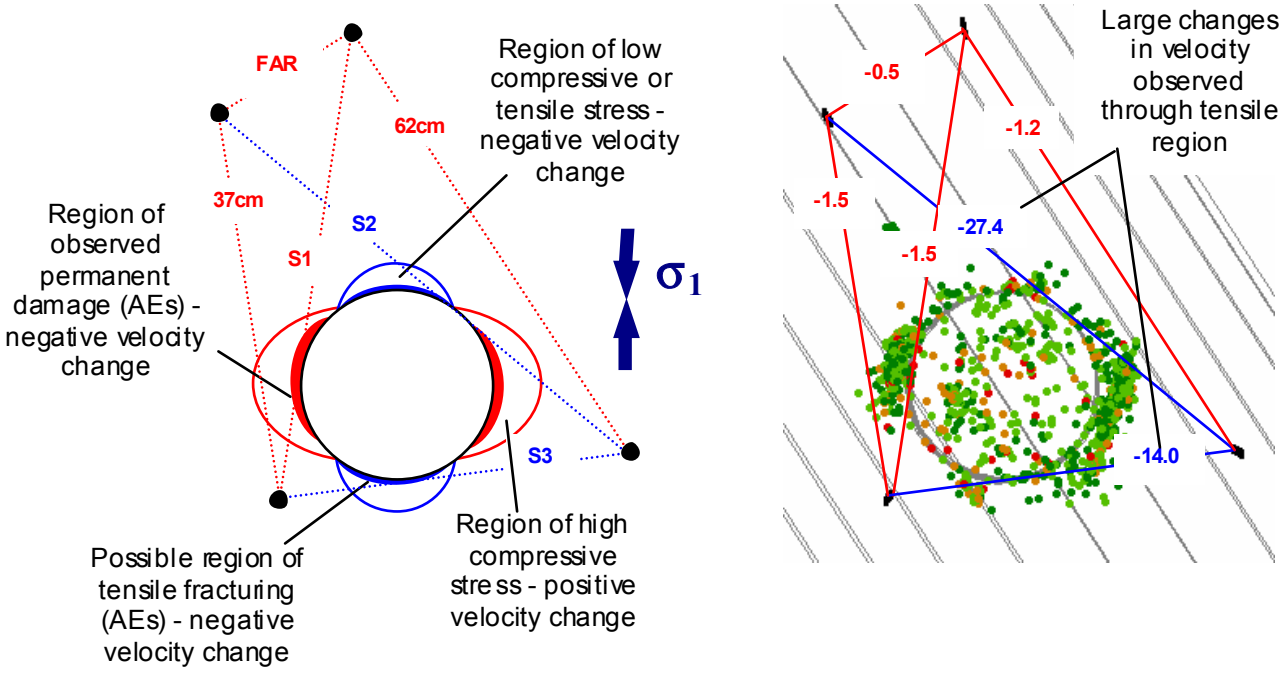

Table of Contents

Acknowledgements

We would like to thank all the staff at the Äspö Hard Rock Laboratory for all of their help. Special thanks for their organisational skills go to Gunnar, Christer Andersson, Åsa and Patrick. Also thanks to Lars-Olof Dahlström for his support, Dave Collins for help in the field and Steve Falls for use of his software.

.

List of Tables

1 Introduction

This report describes results from acoustic emission and ultrasonic monitoring of the excavation of two canister deposition holes in the Prototype Repository at SKB's Hard Rock Laboratory (HRL), Sweden. The Prototype Repository (Figure 1-1) has been designed to simulate a disposal tunnel in a real deep repository for storage of high-level nuclear waste. Its preliminary objective is 'to test and demonstrate the integrated function of the repository components under realistic conditions on a full scale and to compare results with models and assumptions'.

The Prototype Repository consists of a 90m long, 5m diameter sub-horizontal tunnel excavated at 450m depth in a dioritic granite. The tunnel has been excavated using a Tunnel Boring Machine (TBM) and is orientated approximately East to West with a 1.2^{o} inclination in its axis towards its western end. The Prototype Repository design incorporates six canister deposition holes into which will be placed mock waste canisters and a bentonite buffer. The canisters will be heated from within by specially designed electric heaters to simulate stored nuclear material. The tunnel will then be backfilled using a mixture of bentonite and crushed rock, and then sealed using concrete plugs for up to 20 years. Acoustic emission and ultrasonic monitoring is one of a number of scientific measurements that will be used to remotely monitor the performance of the Prototype Repository, and in this case investigates the rock response in the immediate vicinity of two of the deposition holes identified as DA3551G01 and DA3545G01 (Figure 1-1). These were excavated in the period 26th August to 18th September 1999. Each deposition hole has been bored vertically from the floor of the tunnel and measures 1.75m in diameter and approximately 8.8m in length. Excavation was undertaken in eleven 0.8m rounds using a TBM converted for vertical boring.

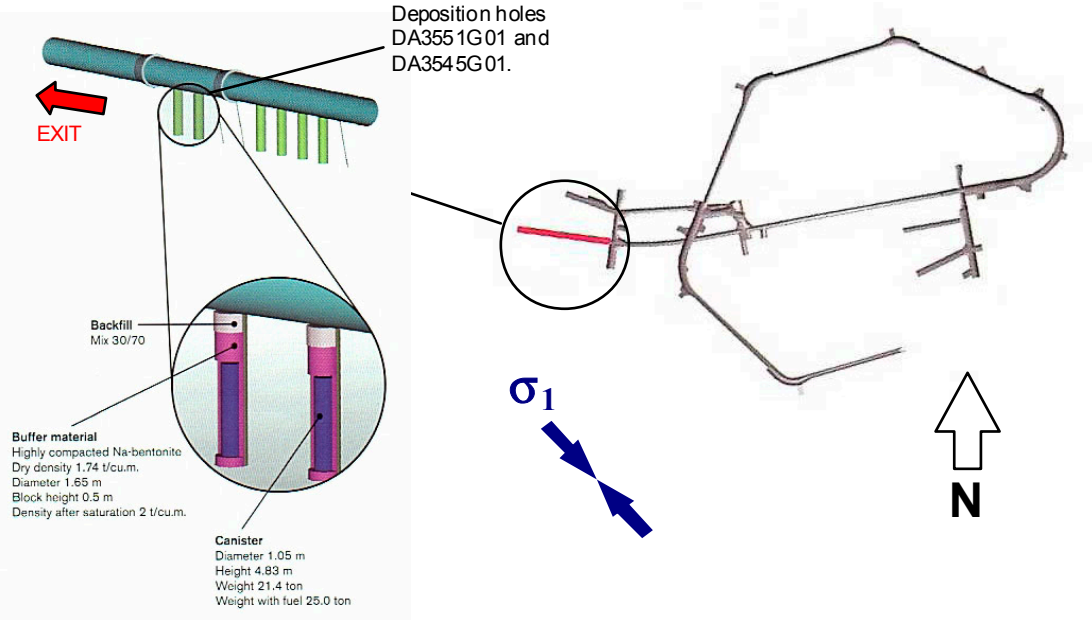

Figure 1-1: *Plan view of the experimental tunnels at the Äspö HRL and the location of the Prototype Repository. A schematic illustration of the final experimental set up is shown with canisters and bentonite clay installed in the two monitored 1.75m diameter deposition holes. Note the entrance of the tunnel is towards the left. Graphics are modified from* SKB*[1999].*

Ultrasonic monitoring has been shown to be an effective tool for observing induced fracturing and the reponse of a medium to applied stresses. *Falls and Young*[1998] gives a review of ultrasonic results from a number of excavation experiments conducted in different underground environments. In recent years hardware and processing software have been developed by the Applied Seismology and Rock Physics Laboratory at Keele University and now by Applied Seismology Consultants Ltd. (ASC), UK specifically for monitoring material changes due to stress-induced damage. Two techniques are utilised using the same monitoring equipment; acoustic emissions and ultrasonic surveying. These techniques have been successfully utilised in a sister experiment to the one reported here [*ASC*, 1999a]. This was conducted at the 420m level in the Canister Retrieval tunnel. The results are summarised in Section 4.1.

Acoustic emissions (AEs) are used to depict the localisation of brittle fracturing on the scale of millimetres in the rock mass. AEs are a time dependent phenomena. In this case, they may occur instantaneously as the deposition hole is excavated due to the method itself or due to the relaxation of the rock mass. They may also occur over a longer period of time due to stresses distributed around the new void inducing new fracturing within the rock or causing disturbance of any pre-existing fractures that may exist. Ultrasonic velocity measurements are used to quantitatively measure the response of the rock over a broader volume and time than the AE scale. Measurements are sensitive to the closing and opening of fractures due to changes in the stress field and due to the accumulation of induced damage within the rock volume. By combining AE measurements, localising the extent of induced damage, and ultrasonic measurements quantifying the degradation of the rock mass, it is possible to measure the overall disturbance induced by both the excavation method and the *in situ* stresses acting on the new void.

2 Experiment Objectives

Acoustic emission and ultrasonic monitoring of the two deposition hole volumes has been conducted in the period 19th August to 29th September 1999 with the following objectives.

- Monitor the background acoustic emission (AE) activity within the deposition hole volume prior to excavation, and perform ultrasonic surveys so as to determine the background ultrasonic velocity in the volume.

- Monitor AE activity immediately after excavation of each deposition hole round and for a period after completion of each deposition hole. Produce accurate source locations for AEs so as to delineate the spatial and temporal extent of brittle microcraking within the surrounding rock mass and the effect of excavation on pre-existing macroscopic fractures.

- Conduct regular ultrasonic surveys during the excavation period so as to observe the ultrasonic response of the rock mass around the deposition hole as excavation commences. In particular this test should use ray paths that skim the perimeter of the deposition hole so as to have a sensitive measure of the excavation response within the immediate rock mass. Use ultrasonic velocities to produce a measure of damage accumulation in this region.

- Relate the AE and ultrasonic measurements to the *in situ* stress regime and modelled excavation induced stresses. Compare the results obtained in the Prototype Repository to those obtained in the Canister Retrieval tunnel at the 420m level.

3 Methodology

3.1 Data Acquisition

The ultrasonic array consists of twenty-four ultrasonic transducers mounted in four borehole sondes (Figure 3-1). Each sonde contains two transmitters and four receivers (Figure 3-2). The sondes are installed in vertical 76mm diameter boreholes approximately 10 meters in length distributed around each deposition hole volume (see Section 3.2 for array geometry). The sondes are fixed to the borehole collars using small bolted steel attachment rods. The sensors are spring loaded against the borehole wall so as to produce good coupling to the rock (Figure 3-1). The transducers respond to the frequency range 35-350kHz.

The piezoelectric transducers operate by converting a transient elastic wave into an electric signal or visa versa. The monitoring system is then operated in one of two modes. The first is used to passively monitor AE activity preferentially within the array volume. AEs release elastic energy in the same way as 'earthquakes' but over a very small scale. At these frequencies AEs have a moment magnitude (M_w) of approximately -6. They occur either during the creation process of new fractures within the medium, or on pre-existing fractures due to small scale movements. Signals from the receivers are first amplified by 40dB and are then captured by an ESG Hyperion Acquisition System controlled by a PC (Figure 3-1). An AE is recorded when the amplitude of the signal on a specified number of channels exceeds a trigger threshold within a time window of 5ms. The system then records the signals from all 16 transducers. In this case a trigger threshold of 50mV on three channels was used. This allows the system to have sufficient sensitivity to record high quality data without recording an abundance of activity that cannot be processed due to very small signal to noise on only a few channels. The captured signals are digitised with a sampling interval of 1µs and a total length of 4096 data points. In general, low noise levels were observed (<2mV) giving high signal to noise and good quality data. Example waveforms from an AE are given in Figure A1.

The second operating mode actively acquires ultrasonic waveforms by scanning across the volume. This allows measurements of P- and S-wave velocities and signal amplitudes over a possible 128 different ray paths. By repeating these ultrasonic surveys at increments in time, a temporal analysis can be obtained for the variation in medium properties. A Panametrics signal generator is used to produce a high frequency electric spike (Figure 3-1). This is sent to each of the 8 transmitters in turn. The signal emitted from each transmitter is recorded over the 16 receivers in a similar fashion to that described above. An external trigger pulse from the signal generator is used to trigger the acquisition system and identifies the transmission start time to an accuracy of one sample point. In order to decrease random noise the signal from each transmitter is stacked 100 times. Example waveforms from an ultrasonic survey are given in Figure A2.

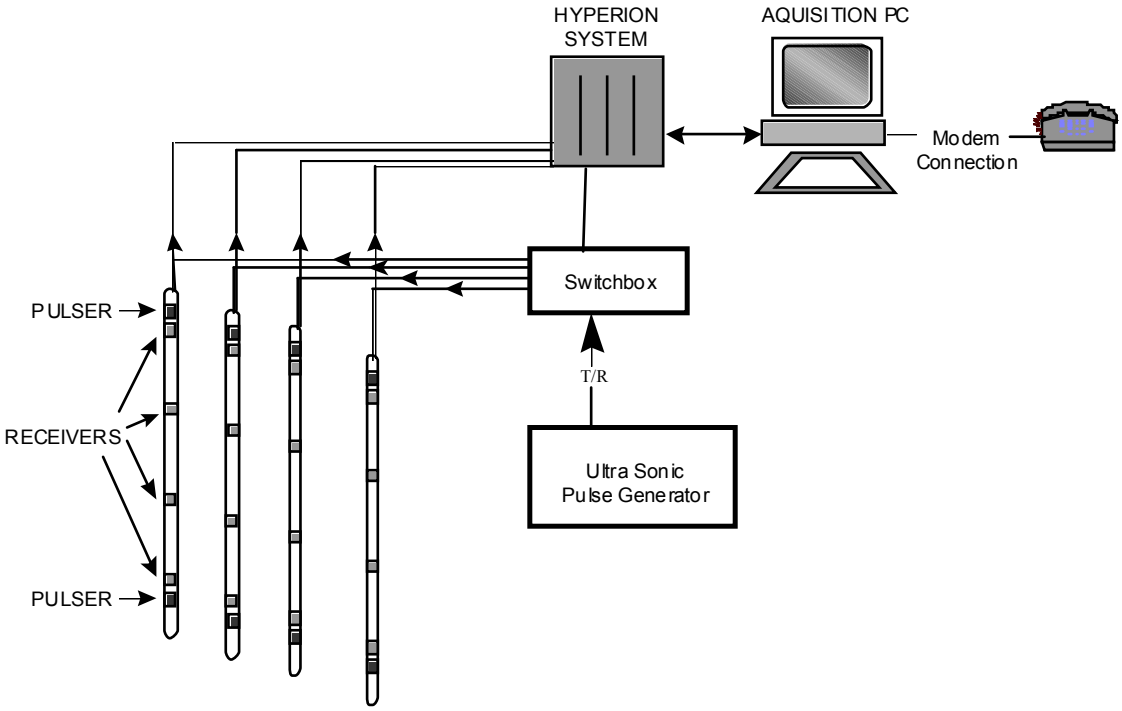

Figure 3-1: *Schematic diagram of the hardware used in the Prototype Repository. The ultrasonic pulse generator sends a signal to each transmitter and the resulting signal is recorded on each receiver. The receivers are also used to listen for AE activity.*

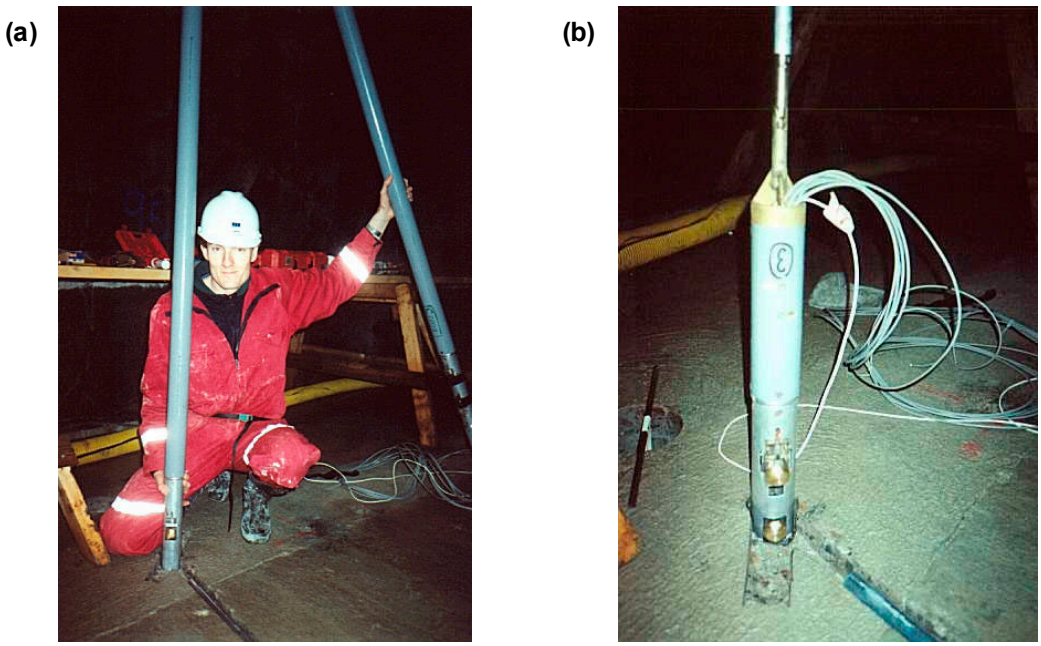

Figure 3-2: *Photographs showing installation of one of the four 8m long borehole sondes used for ultrasonic monitoring in the Canister Retrieval tunnel. Identical installation was performed for the Prototype Repository. Photo b) shows the upper two transducers, the uppermost being a transmitter and the lower a receiver (e.g.figure 3-3) Brass caps are fixed over the transducer faces to give a good coupling to the borehole wall.*

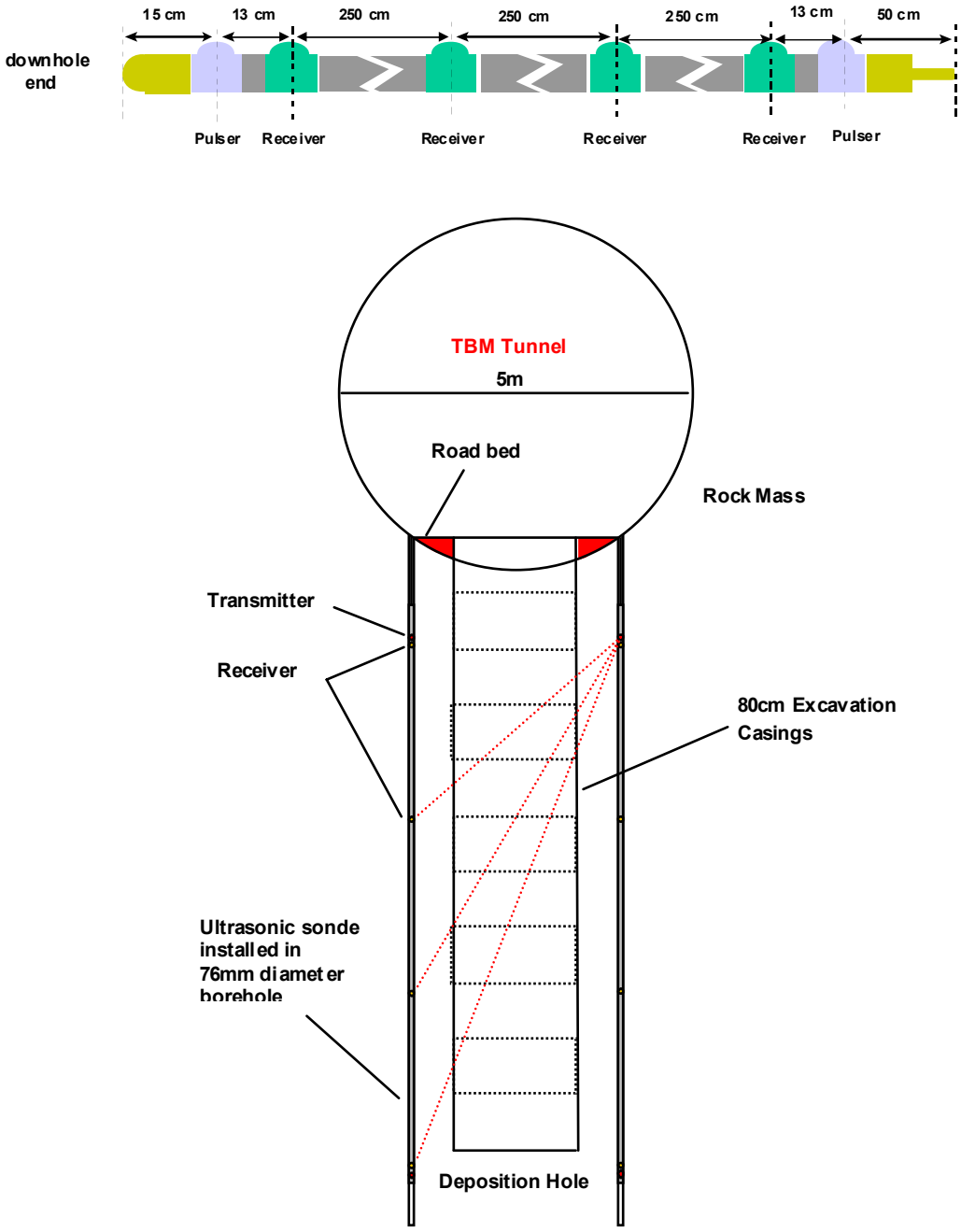

Figure 3-3: Top: Design of the borehole sonde used during ultrasonic monitoring of deposition holes; a transmitter is located at each end of the sonde and four receivers are equally spaced at 2.5m intervals. Bottom: Illustration of the array after installation; sondes are placed in 10m long vertical boreholes. Excavation of the deposition hole is in eleven 80cm rounds. The red arrow indicates the 'passing depth' used in Section 5.4 and defined as the excavation depth at which the deposition hole passes nearest to the shown ray path.

3.2 Array Geometry

The sonde locations for each deposition hole are described in Figure 3-4 and in Table 3-1 and. The array geometry has been designed so as to monitor the complete perimeter of each deposition hole and to produce 'skimming' ray paths during ultrasonic surveys. These ray paths pass within a few centimetres of the deposition hole wall and hence through a region most likely to experience excavation damage. The same four borehole sondes have been used for each array having been re-installed between excavations. Each sonde has been accurately orientated so that the sensor caps point towards the axis of the monitored deposition hole.

Sonde #.	Borehole Ref.	Transmitter #.	Receiver #.
1	KA3553G01	1, 2	1-4
2	KA3551G01	3, 4	5-8
3	KA3548G02	5, 6	9-12
4	KA3548G01	7, 8	13-16

Table 3-1: Location of ultrasonic array for monitoring of deposition hole DA3551G01. See *Figure 3-4* for illustration of array geometry.

Sonde #.	Borehole Ref.	Transmitter #.	Receiver #.
1	KA3543G01	1, 2	1-4
2	KA3545G02	3, 4	5-8
3	KA3548G03	5, 6	9-12
4	KA3548G02	7, 8	13-16

Table 3-2. Location of ultrasonic array for monitoring of deposition hole DA3545G01. See figure 3-4 for illustration of array geometry.

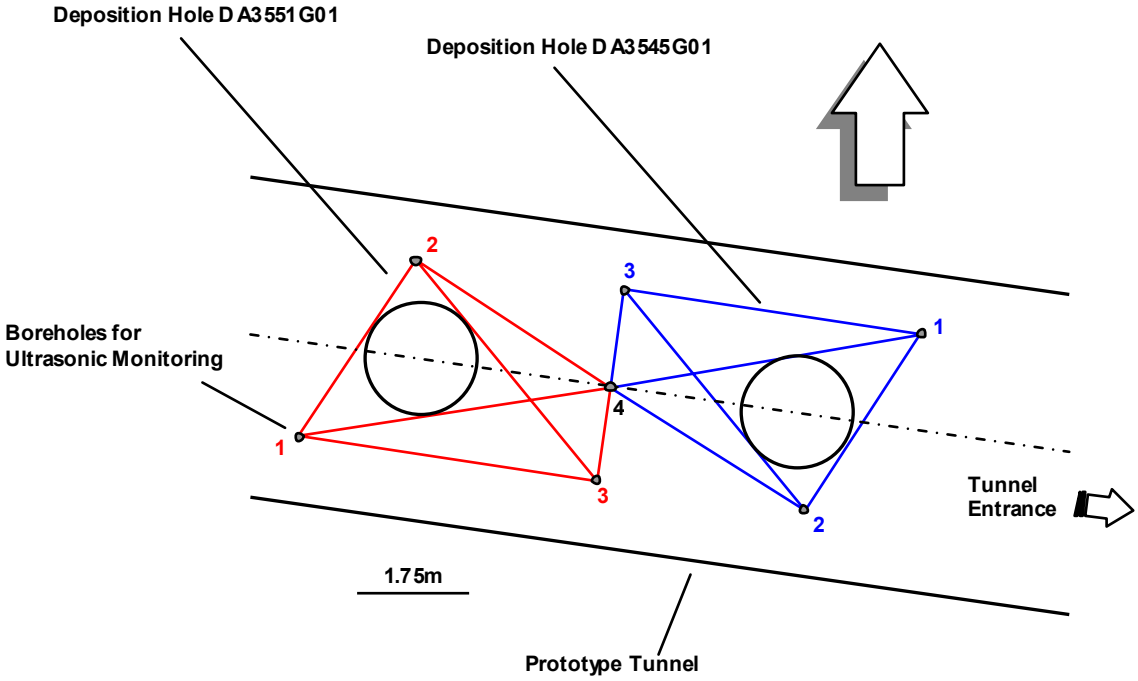

Figure 3-4: *Plan view of the array geometries for the two deposition holes, DA3551G01 and DA3545G01 excavated in the Prototype Tunnel. Red labels are borehole locations for monitoring of deposition hole DA3551G01 labelled by Sonde # (*Table 3-1*). Blue labels are borehole locations for monitoring of deposition hole DA3545G01. Red and blue lines are direct ray paths between sondes illustrating their 'skimming' nature.*

3.3 Monitoring Procedure

Ultrasonic monitoring started at least three days before the start of drilling of each deposition hole, and continued for at least six days after the finish of drilling (Figure 3-5). Monitoring was performed 24 hours per day except during any times of high frequency noise in the rock volume (e.g. deposition hole drilling). During each drilling increment (round), the acquisition system was switched off immediately after the start of excavation and switched on just before the completion of excavation. Immediately after each round a two hour quiet period was observed in the tunnel when no maintenance could be performed on the drilling machine. This period was used for AE monitoring. AE monitoring was also performed overnight between the hours of 2000 to 0600 and during daytime hours when activity on the drilling machine was known due to the system operator being on site.

Ultrasonic surveys were conducted hourly so as to obtain high temporal resolution in the P- and S-wave velocity and amplitude variation along transmitter-receiver raypaths. Surveys were not conducted during deposition hole excavation due to drill noise, and during the first hour of AE monitoring after cessation of drilling.

A calibration survey was performed in each deposition hole so as to analyse uncertainties in AE locations and to calibrate the location algorithm. A mechanical ultrasonic source (Schmidtt hammer) was used in known locations around the deposition hole interior after the completion of excavation. The Schmidtt hammer radiates a high energy signal. In order to test the sensitivity of the array to very small signals, pencil break tests (Section 5.2) were also performed on the interior of each deposition hole.

3.3 Processing Procedure

Data formats and storage procedures are described in *ASC*[1999c]. The raw data are stored as 'events', each being 16 recorded waveforms. The events contain the following data types.

- Microcrack induced acoustic emissions (AEs)
- Ultrasonic survey recordings
- Machine drill noise
- Machine maintenance noise

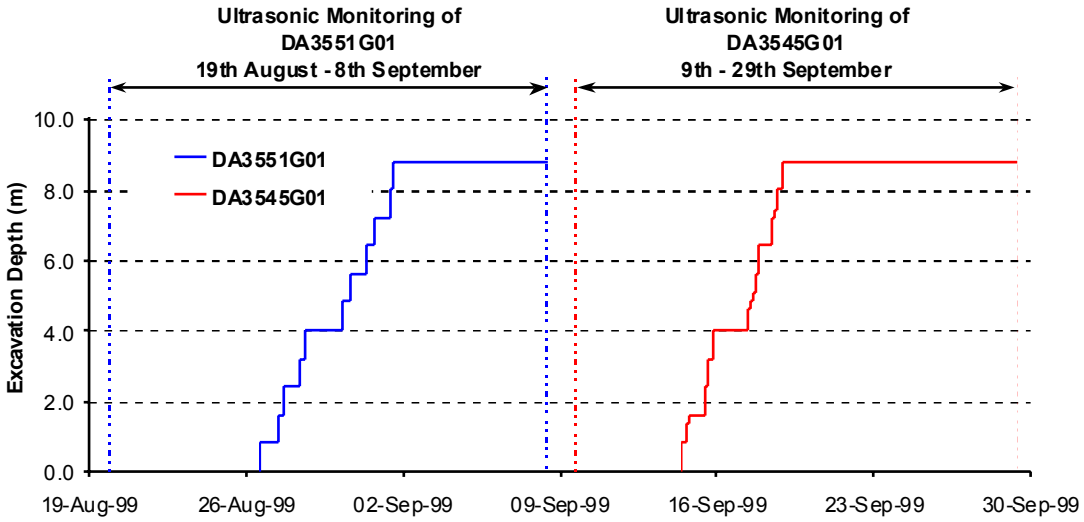

Figure 3-5: *Time chart illustrating the monitoring periods for excavation of the two deposition holes in the Prototype Repository.*

The first stage of the processing is to split these types into individual data sets. The complicating factor in this experiment has been the occurence of significant amounts of machine drill and maintenance events occurring sporadically in time and mixed in with the AE events. It is highly important that this noise is removed so that spurious 'AEs' are not described in the results. To do this the machine data logger was repeatedly synchronised in time with the ultrasonic monitoring system. The time of completion of each excavation round was then logged to an accuracy of approximately 5 seconds. Periods of machine maintenance were also logged. The time of every potential AE trigger was then manually inspected to see if it occurred within a known quiet period when no such noise was occurring. All potential noise was discarded.

AE data and ultrasonic surveys from each deposition hole have then been processed independently and contain the following steps.

Ultrasonic surveys:

1. One survey from each deposition hole is manually picked for P- and S-wave arrival times where possible. The uncertainty in any P-wave time measurement is approximately ±3µs. Velocities are calculated using the time of flight between known transmitter and receiver locations. Uncertainties in P-wave velocity measurements are approximately ±30m.s^{-1}.

2. P- and S-wave arrival times for each hourly survey during the monitoring period are then measured using a cross-correlation procedure. This gives a much more precise measurement of velocity variation than manual processing allows. Thus allowing small (<30m.s^{-1}) velocity changes to be observed. It also allows the efficient processing of large volumes of data. The manually processed survey acts as a reference survey. The

arrivals for every survey are first obtained using an automatic picking algorithm. A data window is then formed around each arrival and the window is then cross-correlated with a similar window from the reference survey. This gives a measurement of the change in arrival time to an accuracy of ±0.2μs. The change in time is then used to calculate a change in velocity with an estimated uncertainty of ±2m.s^{-1}.

3. P- and S-wave RMS signal amplitudes are also obtained from data within a fixed time window around the arrivals.

Acoustic emissions:

1. Calibration surveys are used to optimise an automatic picking and source location algorithm and check location uncertainties.

2. Where possible, P- and S-wave arrival times are measured for each AE using the automatic picking procedure.

3. AEs with ≥6 P-wave arrival times are input into a downhill-simplex location algorithm. This has the option of incorporating either a three-dimensional anisotropic velocity structure or an isotropic structure. Velocities calculated from the ultrasonic surveys are used. It also has the option to constrain locations to lie outside of known voids.

4. Experience from the Canister Retrieval tunnel showed that large source location errors were produced if significant portions of a ray path passed through the excavated deposition hole void. This only becomes a problem for the largest AEs. After preliminary locations were obtained the AEs were reprocessed with these ray paths removed.

5. Spurious AE locations had their automatic picks manually checked. For deposition hole DA3551G01 all automatic picks were manually checked.

4 Acoustic Emissions and Stress Conditions at the HRL

The techniques described in this report have also been performed in a sister experiment conducted in the Canister Retrieval Tunnel at the 420m level [*ASC*, 1999a]. The results from this experiment will be summarised here. It is important when investigating the response of a particular rock mass to excavation to consider the *in situ* stress conditions and the overall rock mass stability. These are summarised for the Prototype Repository.

4.1 Acoustic Emission in the Canister Retrieval Tunnel

In the Canister Retrieval tunnel, two deposition holes (DD0092G01 and DD0086G01) were excavated in a near-identical fashion to those reported here in the Prototype Repository. The tunnel in this case was excavated using a Drill and Blast technique and has a height of approximately 6m. An ultrasonic array was installed around each deposition hole to investigate the response of the rock mass to the excavation. During the entire monitoring period there were a total of 2746 AE triggers. The AE results show regions of intense fracturing located in clusters down the deposition hole wall (e.g. Figure 4-1). These regions are orientated orthogonal to the maximum principal stress at the 420m level. The damaged zone is restricted to approximately 20cm from the deposition hole wall and activity decays rapidly within the first few hours after excavation. The clusters are probably a result of the interaction of induced stresses with excavation through pre-existing features. A linear macroscopic fracture is also imaged. AEs are strongly time-dependent with fracturing being reinitiated around previous rounds when excavation of the deposition hole continues. AEs occur at a much reduced rate (<10 triggers per night) after completion of excavation. These effects are believed to be associated with stress redistribution in the pre-weakened regions.

Ultrasonic surveys give velocities for the pre-disturbed rock mass as approximately 5900m.s^{-1} for P-waves and 3350m.s^{-1} for S-waves. A 3% anisotropy has been imaged. These results are consistent with those obtained in ZEDEX e.g. *Falls and Young*[1996]. The surveys generally describe a drop in velocity during excavation (e.g. ***Figure 4-2***). Observed changes vary from 4m.s^{-1} for ray paths at distance from the deposition hole to sharp drops of 20-30m.s^{-1} for ray paths skimming the deposition hole wall. These variations can be explained using a disturbed and a damaged zone model. As ray paths travel through the disturbed zone, in which induced stresses have preferentially opened or closed pre-existing microcracks, then the ray experiences small increases or decreases in velocity. This results in, for example, a 4m.s^{-1} change observed at distance from the deposition hole. However, ray paths skimming the deposition hole perimeter at 2-3cm distance pass through a region of accumulated damage close to the wall. These then experience a much sharper change in velocity of the order -15m.s^{-1} measured over the entire ray path. This corresponds to a 15% decrease in Young's modulus for the damaged zone.

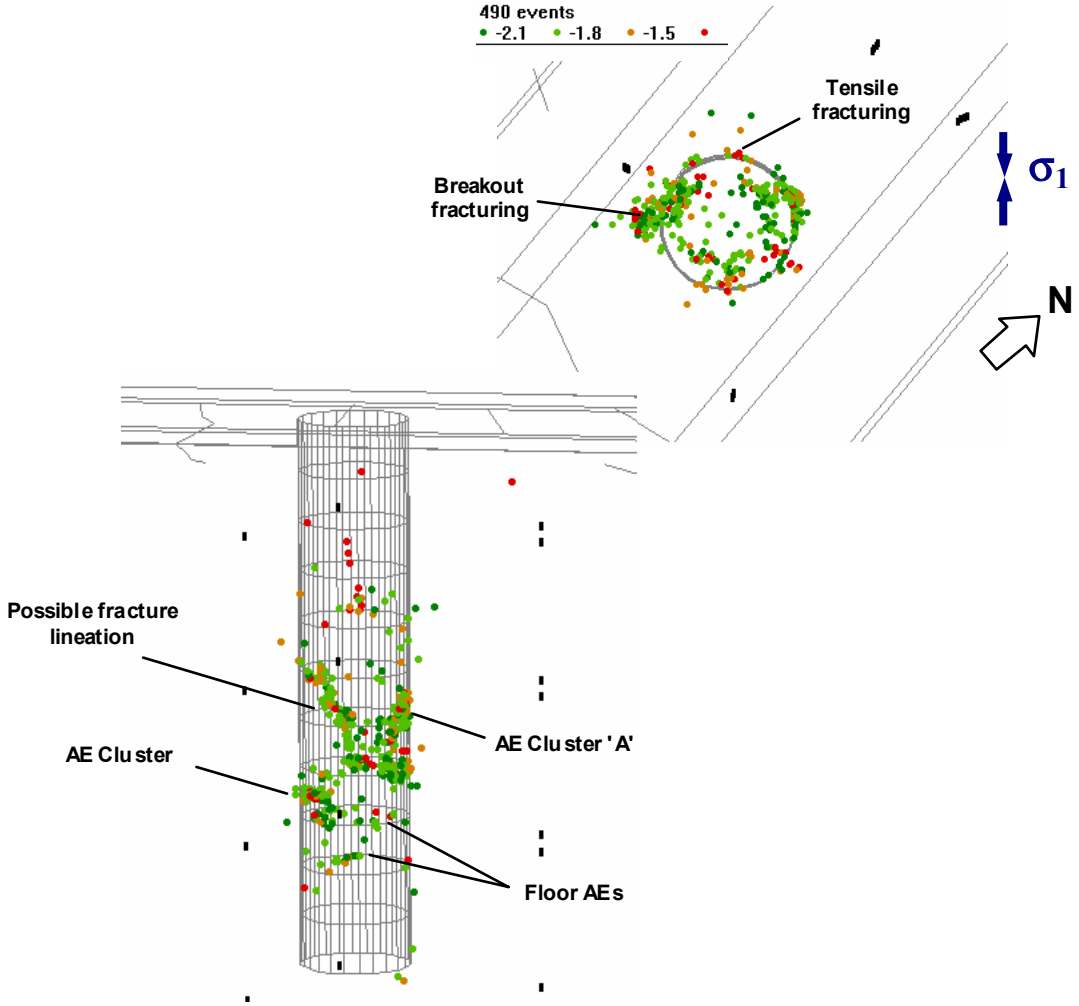

Figure 4-1: *AE locations from excavation of deposition hole DD0092G01 in the Canister Retrieval tunnel.*

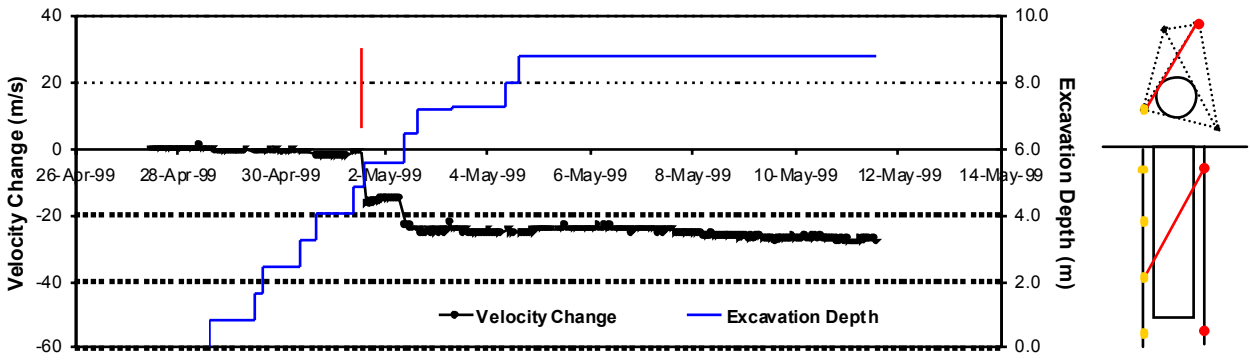

Figure 4-2: *Velocity change for deposition hole DD0092G01 in the Canister Retrieval tunnel measured on the ray path illustrated in the right-hand margin. The red arrow shows the time at which excavation passed the ray path.*

4.2 Stress Conditions in the Prototype Repository

The rock mass at the 450m level is predominantly massive Äspö diorite. *Patel et al.*[1997] have performed detailed mapping of discontinuities in the Prototype Repository tunnel. Two main discontinuous sets of sparse en-echelon fractures were observed. The principal fracture set is steeply dipping orientated to the WNW (Figure 4-3a). This is regarded as the main water-bearing set. Sparsely located fractures are also observed with sub-horizontal dips and with steeply dipping NS orientations. Similar fracture sets were found in the ZEDEX tunnels at the 420m level and are believed to be characteristic of the HRL volume.

Leijon[1995] summarises the stress magnitudes and orientations measured in boreholes at various locations down the HRL ramp using a CSIRO cell. Orientations are summarised in Figure 4-3b. Note there is a strong agreement between the maximum principal stress (σ_1) and the orientation of the principal fracture set. *Young et al.*[1996] note this agreement at the HRL and elsewhere, and use an average *in situ* stress tensor (*Table 4-1*) calculated from the results of *Leijon*[1995] to model stress magnitudes induced around the ZEDEX tunnels. *Young et al.*[1996] analyse stress measurements conducted in the pillar between the two ZEDEX tunnels and relate these to predicted stresses. The authors show that stress magnitudes and orientations are often influenced by the close proximity of fractures to the measurement locations. A relationship that was also observed by *Martin and Chandler*[1993]. *Young et al.*[1996] discount the *in situ* stress results of *Ljunggren and Klasson*[1996] using a Borre Probe on this basis. These results show dissimilar measurements in the ZEDEX volume to that presented by *Leijon*[1995]. AE results in the Canister Retrieval tunnel [*ASC*, 1999a] show damage in the sidewalls of the deposition holes that is consistent with the stress orientations in *Table 4-1*.

Ljunggren and Bergsten[1998] give *in situ* stress measurements from a vertical borehole in the Prototype Repository. Four measurements were performed using a Borre Probe between 20 to 23m distance from the tunnel floor (outside the zone of influence from the tunnel). The mean principal stress magnitudes and orientations are given in *Table 4-2*. These are very similar in magnitude to *Table 4-1*, but are rotated in both azimuth and plunge and are hence out of character with other measurements conducted at the HRL. The reason for this rotation is unclear but may be a result of interference from a neighbouring fracture. In this report, all quoted stress magnitudes and orientations use the same values as that used at the 420m level (*Table 4-1*). It will be shown that the AE results in the Prototype Repository, as in the Canister Retrieval tunnel, are consistent with these stress orientations.

The principal stresses described in *Table 4-1* represent an *in situ* stress ratio of $K=\sigma_1/\sigma_3=3$. The uniaxial compressive strength of the Äspö diorite is approximately $\sigma_c=170$MPa and a uniaxial crack-initiation stress is reported as $\sigma_{ci}=64$MPa. Although stress magnitudes at the HRL are relatively small compared to the strength of the rock the effect of the tunnel in a simple Kirsch solution is likely to increase the maximum compressive stress observed in the floor and roof. *Young et al.*[1996] show modelled maximum compressive stresses reaching >60MPa in the TBM at the ZEDEX volume. There is then an additional effect of stress distribution around the large deposition holes excavated perpendicular to the tunnel. *Zeng and Dahlström*[1999] model a maximum compressive stress of 74MPa in the floor of the Prototype Repository tunnel. The authors use the *in situ* stress measurements of *Ljunggren and Bergsten*[1998]. This is multiplied to 107MPa at the intersection between tunnel and deposition hole and

200MPa when heating begins. Such a multiplication of stresses in this rock type will therefore result in stress-induced fracturing around the perimeter of the deposition holes.

Stress Component	Magnitude (MPa)	Trend (°)	Plunge (°)
σ_1	32	131	0
σ_2	17	41	25
σ_3	10	229	65

Table 4-1: Principal stress values for the 420m level used by *Young et al.*[1996] and originally reported by *Leijon*[1995].

Stress Component	Magnitude (MPa)	Trend (°)	Plunge (°)
σ_1	34	188	39
σ_2	18	94	6
σ_3	13	356	51

Table 4-2: Principal stress values measured in the Prototype Repository [*Ljunggren and Bergsten*, 1998].

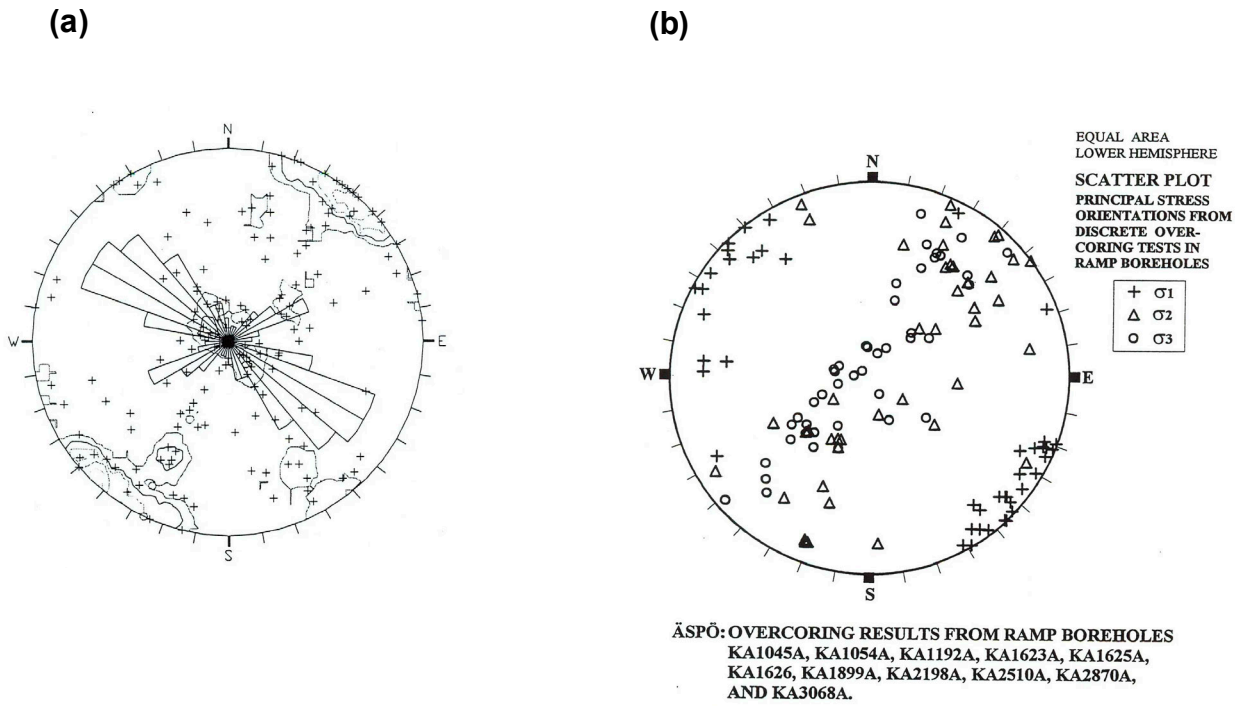

Figure 4-3: a) *Pole, contour and rosette plot of joints from detailed mapping [*Patel et al.*, 1997]*. ***b)*** *Principal stress orientations measured from boreholes excavated from the HRL ramp [*Leijon*, 1995]*.

5 Results from Ultrasonic Monitoring

5.1 Ultrasonic Velocity Structure

Reference ultrasonic surveys have been chosen from the period before excavation began for each deposition hole so as to obtain a measure of the background velocity structure. P- and S-wave velocity measurements for deposition hole DA3551G01 are shown in the lower-hemisphere stereonets of Figure 5-1. The mean P-wave velocity is 5988m.s^{-1} over 70 ray paths. The scale range in this plot is 5740-6100m.s^{-1} and each colour increment varies by the estimated uncertainty in any one measurement (30m.s^{-1}). The mean S-wave velocity is 3392m.s^{-1}. There is very little variation in the measurements over the lower hemisphere that cannot be explained by measurement uncertainty. This indicates the rock mass is ultrasonically isotropic and homogeneous. This contrasts with results from the Canister Retrieval tunnel where a 3% anisotropy was observed and the mean P-wave velocities were approximately 80m.s^{-1} lower. S-wave velocities are also observed to be higher in the Prototype Repository.

Figure 5-2 shows similar plots for deposition hole DA3545G01. Again, no anisotropy is observed giving consistent results to that for the first deposition hole, although mean velocities are slightly higher at 6013 and 3397m.s^{-1} for P- and S-waves respectively. These results suggest the rock type experienced in the Prototype Repository differs slightly to that experienced at the 420m level. It is well recognised that the Äspö HRL experiences a mixture of dioritic compositions, varying in chemistry and grain sizes. This probably leads to the difference in velocity measurements.

5.2 Acoustic Emission Locations

A total of 387 AE triggers occurred during excavation of deposition hole DA3551G01 and 2080 during excavation of deposition hole DA3545G01. There were hence significantly more triggers during the second hole to be excavated compared to the first. Figure 5-3 shows the trigger rate for excavation of the two deposition holes. For DA3551G01 the vast majority of triggers occurred during the first 3 rounds where trigger rates got above 20 events per hour. After these rounds, trigger rates dropped and rarely reached >10 events per hour. In comparison, the second deposition hole had similar trigger rates in the first few rounds reaching approximately 30 events per hour. However, after round 5 trigger rates increased significantly to a peak of 150 events per hour after round 10. There are a number of plausible explanations for this disparity. These will be explored in the following section.

(a)

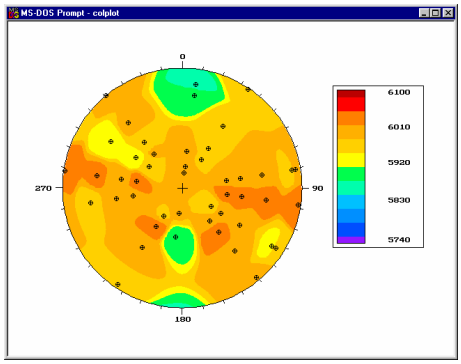

(b)

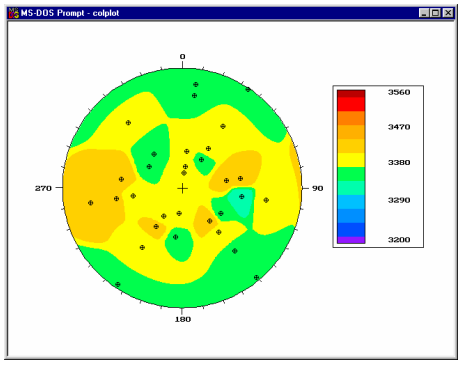

Figure 5-1: *Measured ultrasonic velocities from the reference survey for DA3551G01 shown on a lower-hemisphere stereonets. The survey used is 24th August at 01:00.* ***a)*** *P-wave velocities.* ***b)*** *S-wave velocities.*

(a)

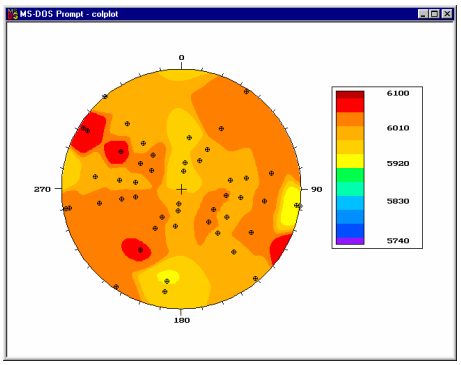

(b)

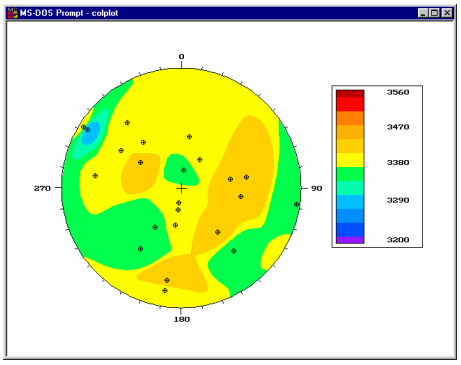

Figure 5-2: *Measured ultrasonic velocities from the reference survey for DA3545G01 shown on lower-hemisphere stereonets. The survey used is 13th September at 01:00.* ***a)*** *P-wave velocities.* ***b)*** *S-wave velocities.*

To test the source location accuracy of the array geometry a set of calibration shots were performed around the deposition hole. These utilised a Schmidtt hammer as an ultrasonic source. Locations for the Schmidtt shots are shown as red markers in Figure A3 and compare well with true locations calculated from survey points on the tunnel floor (green markers). From experience gained in the Retrieval Tunnel it was observed that this source is lower frequency and much higher magnitude than the real AEs recorded around the deposition hole. In order to test the sensitivity of the array to very small magnitude events a pencil lead source was also used at points around the interior of the borehole. Pencil lead breaks are often used as standard calibration sources for ultrasonic transducers in the laboratory (e.g. *Breckenridge et al.*[1990]). The method uses a breaking 0.5mm HB lead from a Pentel ratchet pencil orientated at approximately 45^{o} to the deposition hole surface. In a laboratory sample of a few centimetre dimensions such a source is regarded as high magnitude. In the case of deposition hole monitoring however, where source-receiver distances are often >2m, it is a very low magnitude source. In both deposition holes, pencil lead breaks were recorded on sufficient numbers of transducers to allow locations to be computed (Figure A4). Again these compare very well with locations calculated from survey points on the tunnel floor. These tests give confidence in computed AE source locations with maximum estimated errors being approximately 10cm.

The pencil lead tests also allow an estimate of the scale of cracking that AEs represent. Although at present it is not possible to directly compute AE source dimension from recorded waveforms, the fact that pencil lead tests can be recorded at all indicates that the array can record cracking down to millimetres in dimension. The processing currently employed gives a magnitude (M_u) calculated from waveform amplitudes and is a logarithmic scale similar to other magnitudes calculated in seismology. This scale is not calibrated to a seismological scale such as moment magnitude (M_w). AE magnitudes computed around the deposition holes are generally in the range $-2.3 < M_u < -1.0$. The pencil lead tests are at the lowest end of this scale in the range $-2.3 < M_u < -2.2$ and represent failure on a source region of approximately 1mm. The ultrasonic system is hence able to record AEs from fractures that are of the order of millimetres; approximately the grain size of the rock.

AE locations from monitoring of both deposition holes are shown in Figure 5-4. In plan view there is a clear clustering of events in the NE-SW quadrants of the two deposition holes. Both holes are consistent, although the first hole has significantly lower numbers of located AEs. In total 1153 AE locations have been computed, of which 269 occurred during monitoring of DA3551G01 and 884 during monitoring of DA3545G01. The distribution of events with azimuth around the deposition hole is highlighted in Figure 5-5 and is approximately orthogonal to the maximum principal stress given in *Table 4-1*. The distribution therefore lies in regions of high compressive stress given by a simple Kirsch solution and locates where breakout damage would be expected. Figure 5-6 shows an event density plot for the deposition hole DA3545G01. Any deviation of this distribution from normal to the σ_1 direction is within $\pm 15^{o}$ azimuth. These results are consistent with the AEs located around deposition holes in the Retrieval Tunnel [*ASC*, 1999a], but are not consistent with *in situ* stress orientations measured in the Prototype Tunnel [*Ljunggren and Bergsten*, 1998]. The relationship between AE numbers and distance into the sidewall of each deposition hole is shown in Figure 5-7. For DA3551G01, 88% of the AEs locate within the first 20cm and 95% within the first 30cm. For DA3545G01 these values are 70% and 88%. A good approximation of the

extent of the damaged zone is then 20-30cm. This is consistent to that observed in the Retrieval Tunnel.

AEs locate down the full length of both deposition holes (Figure 5-4). For DA3551G01 the locations are concentrated in the upper few rounds and decrease in numbers with depth (Figure 5-7a). The AEs are not continuous down the borehole length but instead locate in discrete clusters as was observed in the Retrieval Tunnel. This phenomenon is more noticeable in deposition hole DA3545G01 where extensive clustering is observed, particularly in the lower half of the deposition hole. In this case AE locations increase as the excavation depth is increased (b). The highest numbers of AEs, and hence the greatest damage, is observed around the four deepest rounds. The time dependency of the AE locations is shown in Figure 5-8. The majority of AEs locate within 24 hours of the excavation passing a certain depth. However, AEs locate down the length of the excavation for many days, particularly in clustered regions where damage is probably more extensive. Two clusters labelled A and B are highlighted in both Figure 5-4 and Figure 5-8. At the end of the monitoring period AEs are still occurring down the length of the deposition hole although the rate of triggering has dropped to <10 events per night (Figure 5-3). This clustering in both space and time is likely to be associated with excavation through pre-existing fractures.

Figure 5-1 shows AEs from the lower rounds of deposition hole DA3545G01. Breakout fracturing is highlighted. This occurs in intense clustering extending for approximately 2m across rounds 8, 9 and 10. AE clusters are also observed sporadically down the length of the deposition hole in regions parallel to the maximum principal stress. These occur in regions of very low compressive stress or possibly tensile stress (if the stress ratio, K>3). It is possible these tensile clusters occur on intersections between the deposition hole and pre-existing macroscopic fractures. In this case the fracture acts as a weakness in the rock mass upon which increased AE activity can occur. Also, shown is a small AE cluster of four located events. The cluster locates at approximately 0.8m from the deposition hole wall. The AEs are all of small magnitude, however their arrival times have been checked manually and there is a large confidence in the locations. These AEs are the only examples recorded during monitoring of all four deposition holes in both the Prototype and Retrieval Tunnels where AEs locate at significant distances from the deposition hole wall. They occur after excavation of round 10. They are probably associated with slip on a pre-existing fracture caused by stress redistribution as the excavation face passes by.

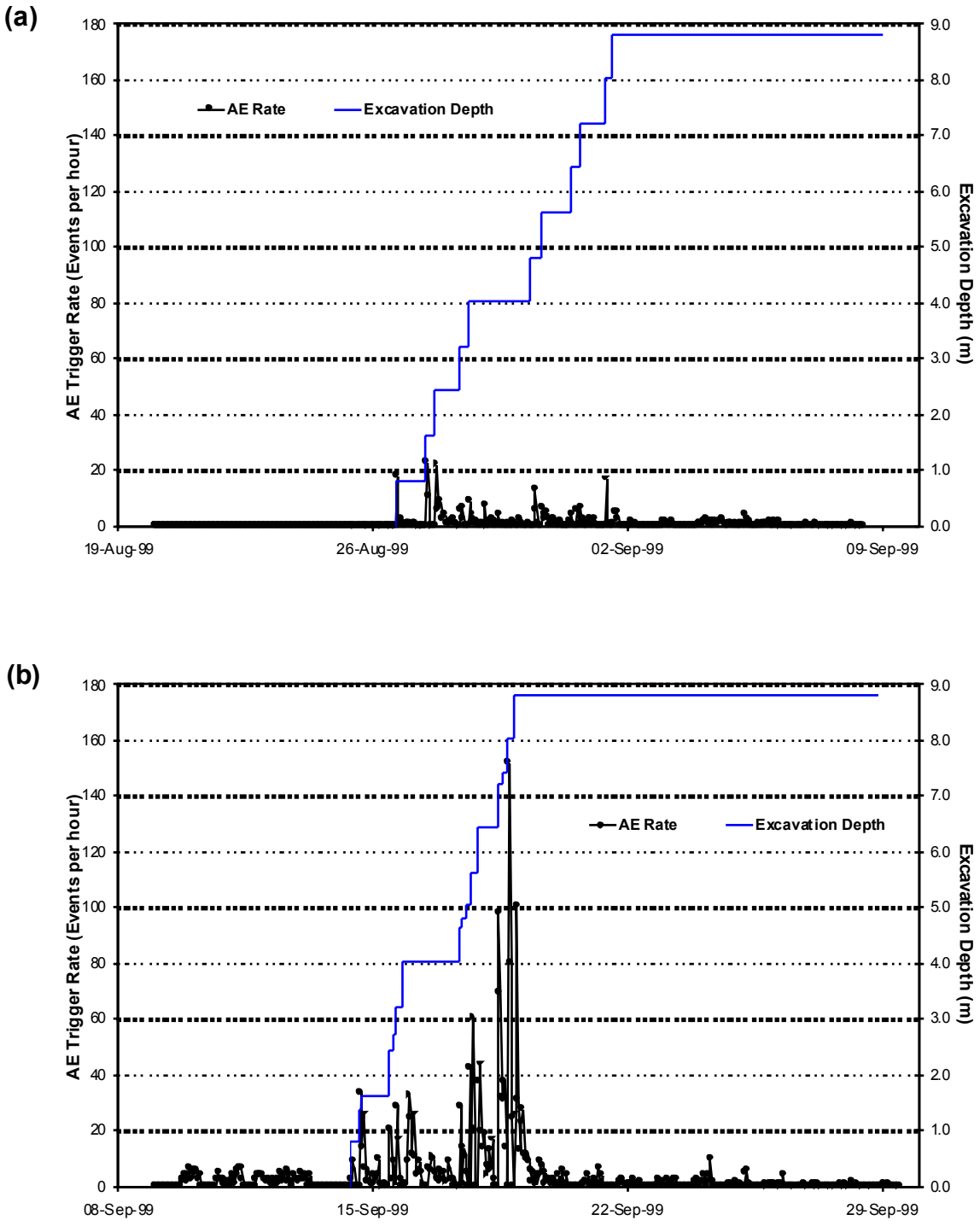

Figure 5-3: *AE trigger rate through the monitoring periods for the two deposition holes: a) DA3551G01 and b) DA3545G01. Also shown is the excavation depth for each deposition hole.*

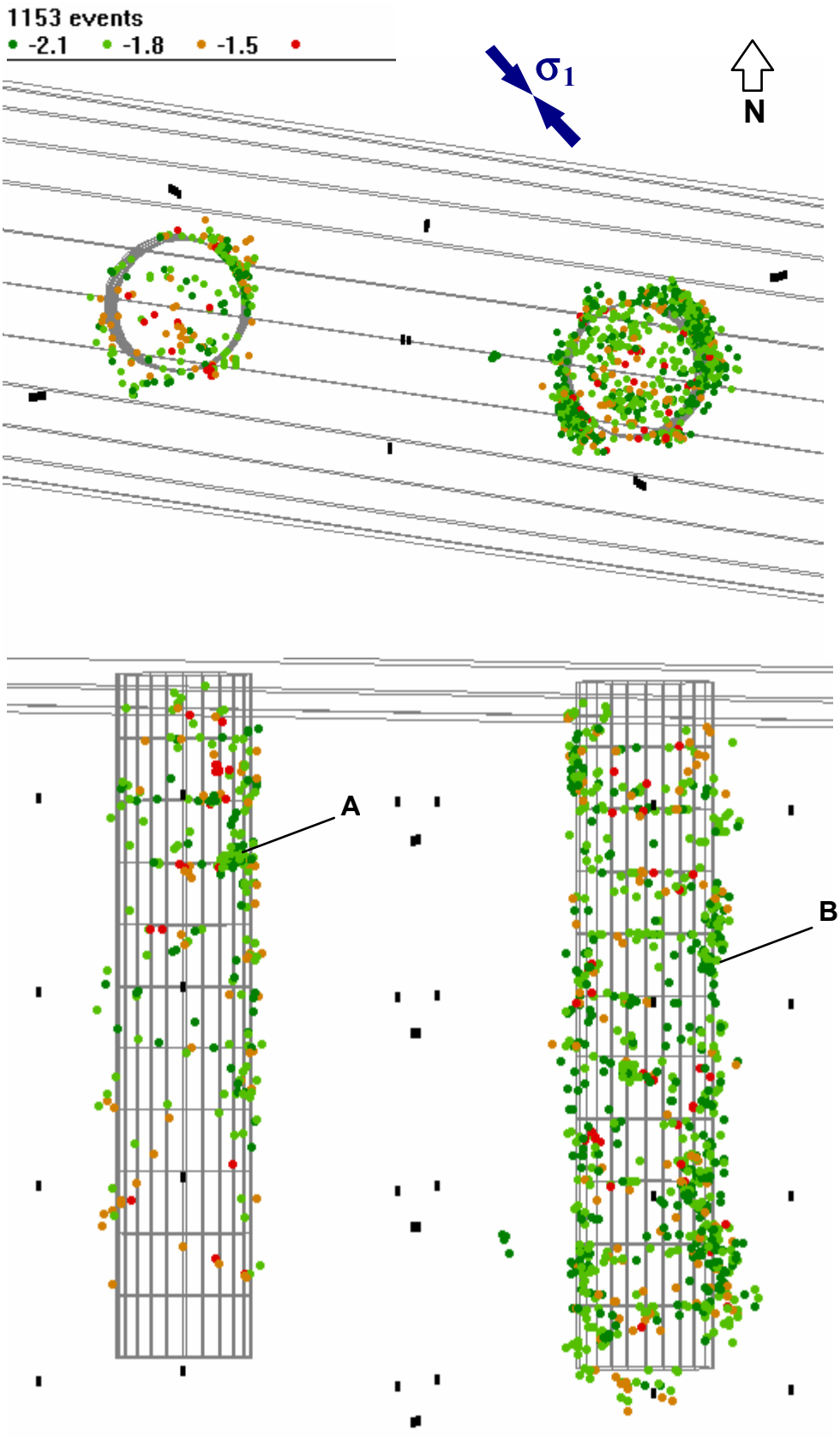

Figure 5-4: *All AE locations obtained from monitoring of both deposition holes DA3551G01 and DA3545G01 in the Prototype tunnel. Events are colour scaled to their ultrasonic magnitude. Upper plot is in plan, lower plot is in cross-section. Black markers indicate transducer locations.*

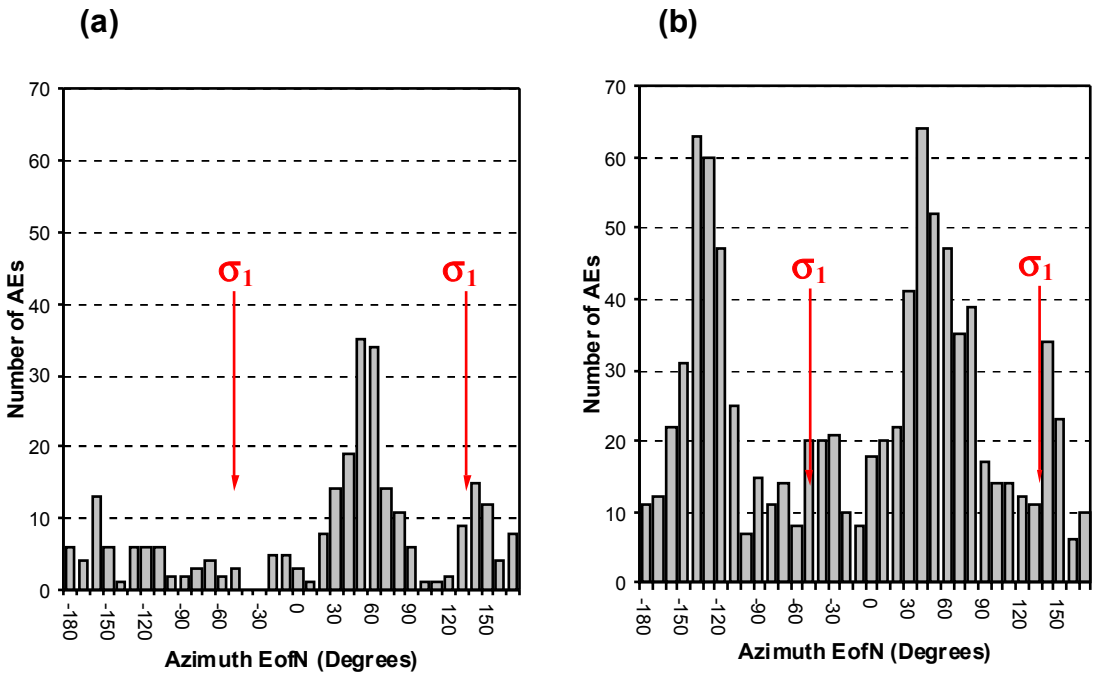

Figure 5-5: *AE distribution with azimuth around each deposition hole: a) DA3551G01 and b) DA3545G01. The red arrows indicate the azimuth of* σ_1 *from* Table 4-1.

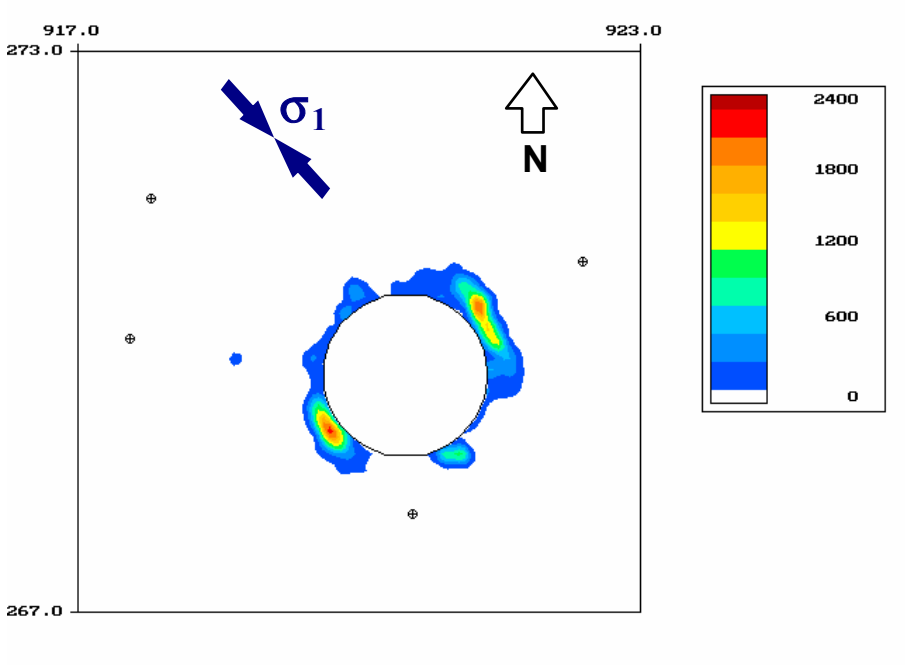

Figure 5-6: *An event density plot (plan view) for deposition hole DA3545G01. Also shown is the* σ_1 *direction from* Table 4-1. *Units are interpolated numbers of AEs per* m^2.

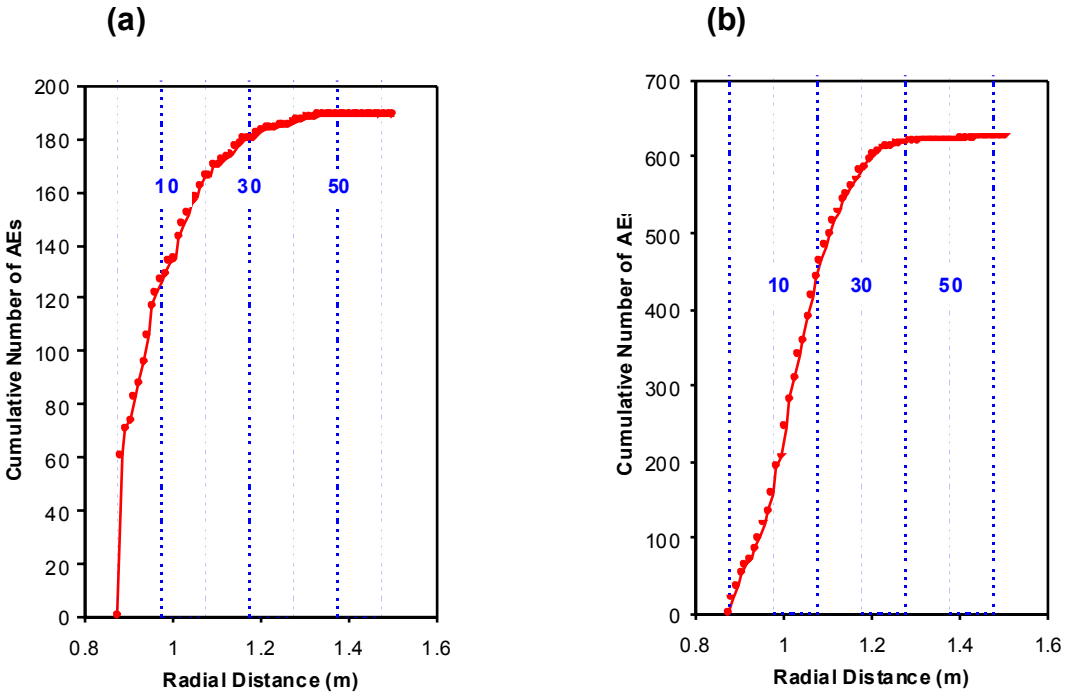

Figure 5-7: The cumulative number of AEs with radial distance from the deposition hole wall: a) DA3551G01 and b) DA3545G01. Blue dashed lines and labels indicate distance from the wall in centimetres.

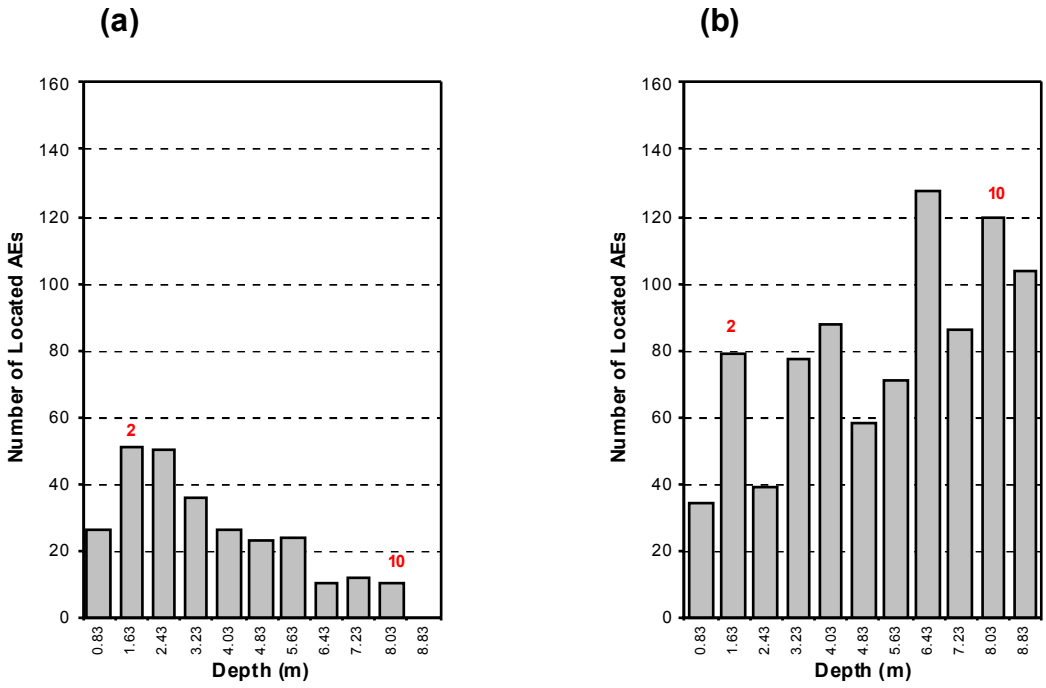

Figure 5-8 *Distribution of AE locations with depth. Each depth increment represents one round measured from the steel road bed. Rounds 2 and 10 are marked.*

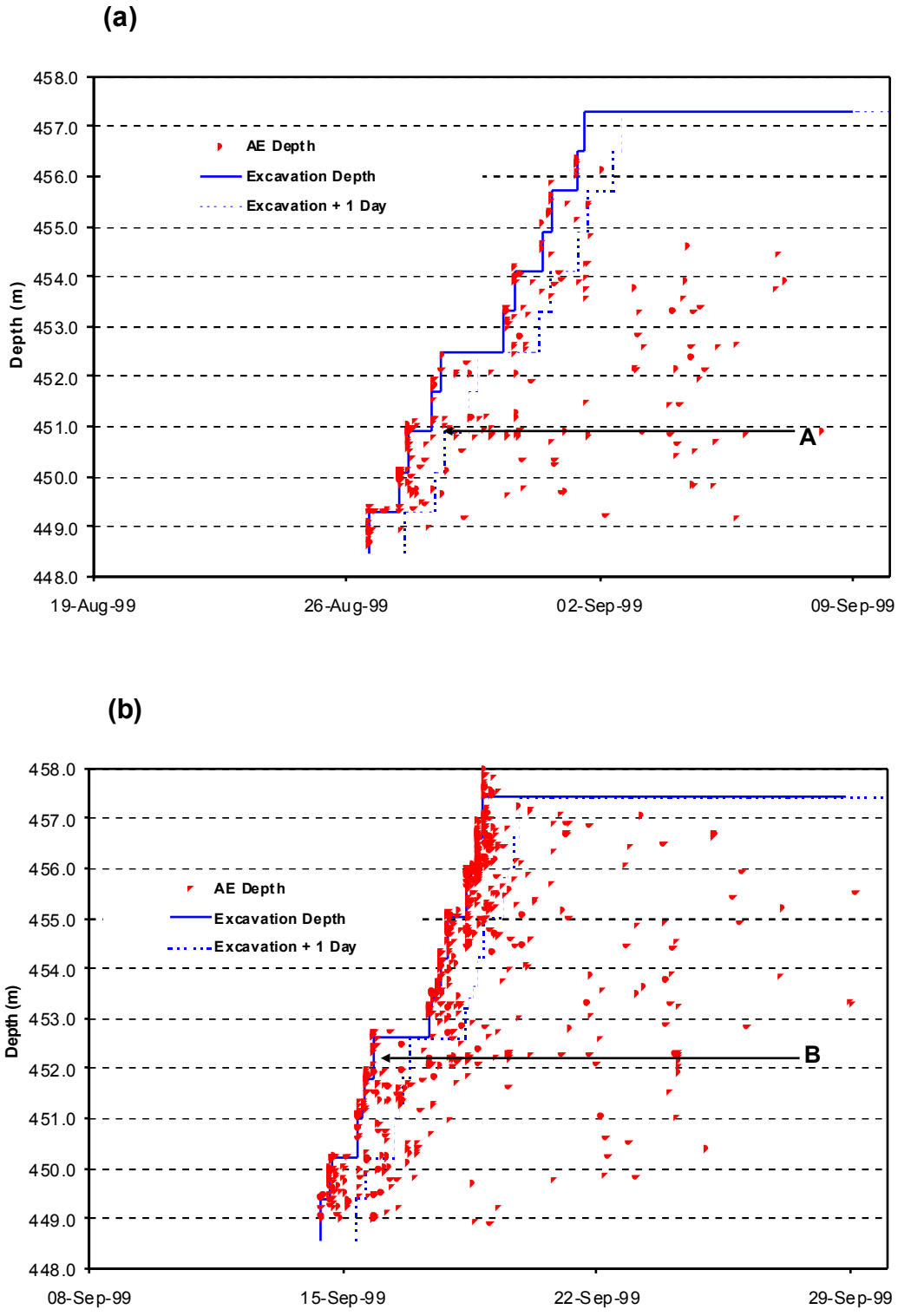

Figure 5-9: *Acoustic emission time dependency for* ***a)*** *DA3551G01 and* ***b)*** *DA3545G01. Red markers are AE depths with time. The solid blue line is the excavation depth and the dashed blue is the excavation depth displaced by 24 hours. Two time-dependent clusters are noted as A and B.*

5.3 Acoustic Emission Numbers

There is an obvious difference in the number of AEs located around each deposition hole. The located AEs are a function of the number of triggers recorded by the acquisition system and the processing techniques used. The acquisition system settings were identical during monitoring of both deposition holes and identical to the monitoring performed in the Retrieval tunnel. During monitoring of DA3551G01 the small data flow compared to that observed in the Retrieval tunnel was observed. The acquisition system triggering was sporadically checked. Trigger thresholds and number of triggering channels were lowered to check the sensitivity of the array to very small AEs. No significant increases in data were observed resulting in the conclusion that AEs were not occurring in the same abundance during excavation of DA3551G01 as seen in the Retrieval tunnel.

As the number of triggers obtained during excavation of DA3551G01 was small, it was felt that the number of well-constrained AE locations had to be maximised to give an accurate picture of fracturing occurring around the deposition hole. All automatic time picks were therefore manually checked. Although this is far more time consuming than relying on purely automatic locations it produces a higher quantity of location data to analyse (*Table 5-1*). Based on the experience gained from monitoring in the Retrieval Tunnel, processing of DA3545G01 also included a manual element. The automatic picks for locations with high errors were manually checked. This reduces the effect of the tunnel void and reduces the scatter in the locations, giving a clearer location picture. Figure A5 tests differences in array and processing sensitivities.

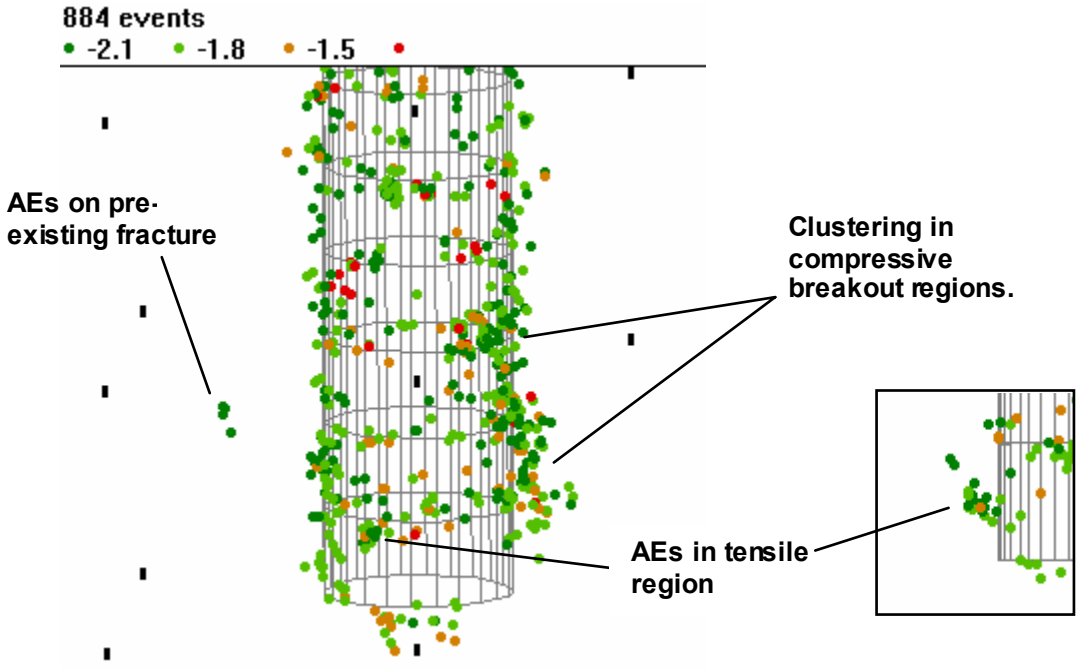

Figure 5-10: *Locations for all AEs in the lower rounds of deposition hole DA3545G01. Markers are colour scaled to ultrasonic magnitude.*

The b-values calculated from this figure represent the ability of the acquisition array, monitoring system and processing techniques to locate events of different magnitudes. The b-values for deposition holes DA3551G01, DA3545G01 and DD0086G01 are almost identical (*Table 5-1*) and show that all three AE data sets have the same relative proportions of small events to large events even though slightly different processing techniques were used in the three deposition holes. The b-value for DD0092G01 is much reduced and represents an increase in larger events relative to smaller ones. However, the threshold of the lowest magnitude events is the same. This effect may be related to the large macroscopic fracture that was dominant in this deposition hole [*ASC*, 1999a] causing higher numbers of larger events.

Tunnel	Deposition Hole	AE Triggers	AE Locations	% Located	b-value
Retrieval	**DD0092G01**	1531	490	32%	0.58
Retrieval	**DD0086G01**	1215	401	33%	0.77
Prototype	**DA3551G01**	387	269	70%	0.74
Prototype	**DA3545G01**	2080	884	43%	0.76

Table 5-1: Differences in total numbers of AE triggers and locations for monitoring of deposition holes in the Retrieval and Prototype tunnels. 'b-values' are taken from *Figure A5*.

In summary, the evidence given above suggests that the transducer array, acquisition hardware and processing techniques do not cause sensitivity differences between the deposition holes, particularly in the Prototype Tunnel. The differences in the number of triggers observed between the two deposition holes, in this case, must therefore be due to the rock mass response. There are a number of plausible reasons why the activity may be higher in the second hole to be excavated (DA3545G01). The true reason may be a combination of these.

Change in rock structure. It is unlikely that there is a change in rock type between the two deposition holes that is significant enough for such a large change in AE activity to occur. However, it is possible that the second hole is intersected by a much larger number of pre-existing fractures and/or these fractures are orientated in a preferential manner to increase AE activity. If so these fractures have a significant bearing on the amount of damage induced in a particular deposition hole.

1) Stress transfer. It is possible that the excavation of a deposition hole changes the stress regime around the tunnel above it and around a deposition hole then excavated close to it. The excavation of one deposition hole therefore has an effect on a subsequent deposition hole. If this stress change was large enough then it may increase the amount of damage observed around the second deposition hole. Such an observation was also noted in the Retrieval Tunnel.

2) Excavation differences. If there were any differences in the excavation method such as rate of excavation, pressure of the cutter head, or some additional damage induced into the side wall then this may have the effect of weakening the rock mass. This pre-weakened rock mass is then more prone to stress-induced damage.

The clustered nature of AE locations observed in deposition hole DA3545G01 (Figure 5-4), and particularly those observed in DD0092G01 in the Retrieval Tunnel, suggest that intersecting pre-existing fractures may have a strong link with the number of AEs observed. Reason (1) above may therefore be the dominating factor.

5.4 Change in Ultrasonic Properties During Excavation

Velocity changes are measured between transmitter-receiver pairs using a cross-correlation technique that allows a velocity resolution of $\pm 2 m.s^{-1}$. Very consistent velocity changes were observed between the two deposition holes in the Prototype Tunnel. These also agree with observations from the Retrieval Tunnel (summarised in Section 4.1). For each deposition hole the array geometry is such that in plan view there are six possible ray path categories illustrated in Figure 5-11. Three of these ray path categories 'skim' the deposition hole wall at approximately 2-3cm. Velocity changes measured on transmitter-receiver pairs for one of these ray path categories (S3) are shown in Figure 5-12 and Figure 5-13 for deposition hole DA3551G01 and Figure 5-14 and Figure 5-15 for DA3545G01. There is generally little velocity change until the deposition hole passes the ray path (red arrow). There is then an abrupt change of between -10 to $-30 m.s^{-1}$. This may occur over 1-3 consecutive rounds and indicates a progressive opening of fractures along the ray path as the excavation passes. Ray paths that do not show such changes (Figure 5-13d and Figure 5-15d) travel underneath the excavation and do not effectively pass the deposition hole. Both P- and S-waves show similar trends in velocity change (e.g.Figure 5-13a) although the magnitude often differs. Comparing each plot in the four figures shows a very consistent trend in velocity change for the S3 ray path category between the two deposition holes.

Each ray path category differs in the magnitude of the observed velocity change. *Figure 5-16* shows average changes in velocity computed for each of the ray path categories and superimposed on the AE locations. Of the six ray path categories two (S2 and S3) show consistently high negative velocity changes of -14 to $-27 m.s^{-1}$. The other four categories describe only small changes of +1 to $-4 m.s^{-1}$. The most significant of these is S1. Even though this category skims the deposition hole wall, average changes of only -4.2 and $-1.5 m.s^{-1}$ are observed for the two deposition holes. These velocity changes observed in the Prototype Tunnel are consistent with a damaged and disturbed zone model proposed for velocity changes observed in the Retrieval Tunnel [*ASC*, 1999a].

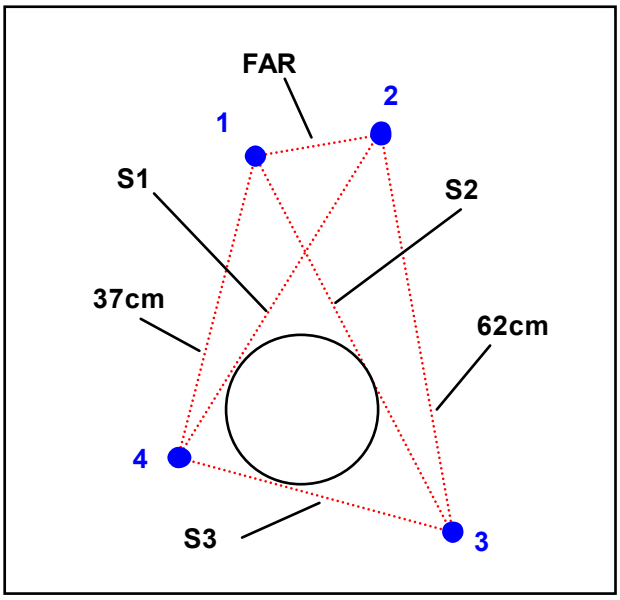

Figure 5-11: *The six ray path categories in cross-section (plan view). Blue markers indicate the locations of the four ultrasonic sondes. Note that in three dimensions there are 128 possible ray paths between all of the transmitters and receivers down the four sondes. Of the six categories there are three sets of skimming ray paths labelled 'S1', 'S2' and 'S3', two sets of ray paths passing at greater distances labelled '37cm' and '62cm'. The final ray path type (labelled 'FAR') does not effectively pass the deposition hole but travels through the rock mass at approximately 1.5 deposition hole diameters.*

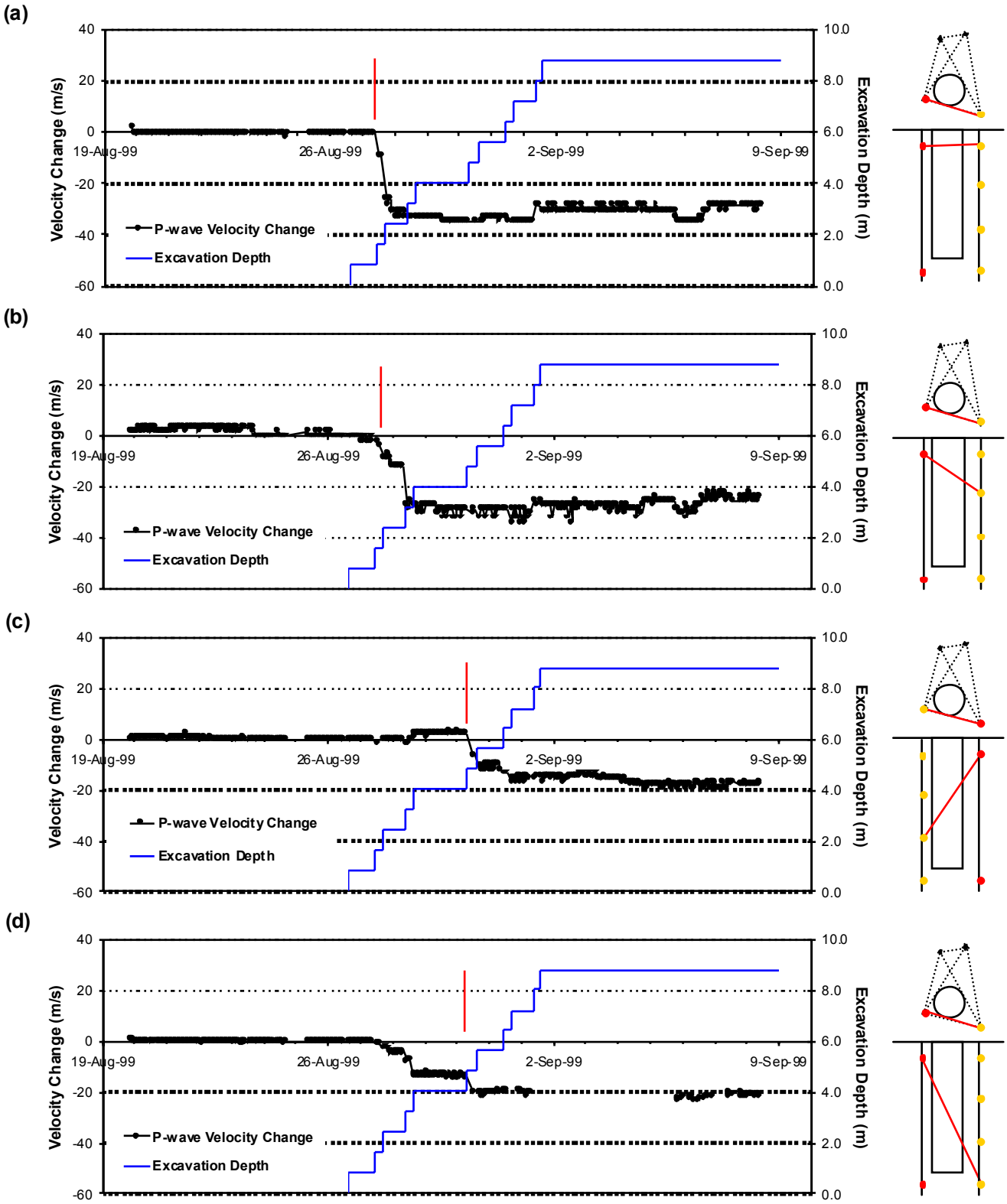

Figure 5-12: Velocity changes measured on ray path category 'S3' (Figure 5-11) for deposition hole DA3551G01. Ray paths shown are from a top transmitter to receivers with increasing depth: a) transmitter, t_n=3, receiver, r_n=1; b) t_n=3, r_n=2; c) t_n=1, r_n=7; d) t_n=3, r_n=4. Schematic diagrams in the right margin indicate the relative locations of transmitter (red) and receiver (gold). The red arrow indicates the passing depth defined in Figure 3-3

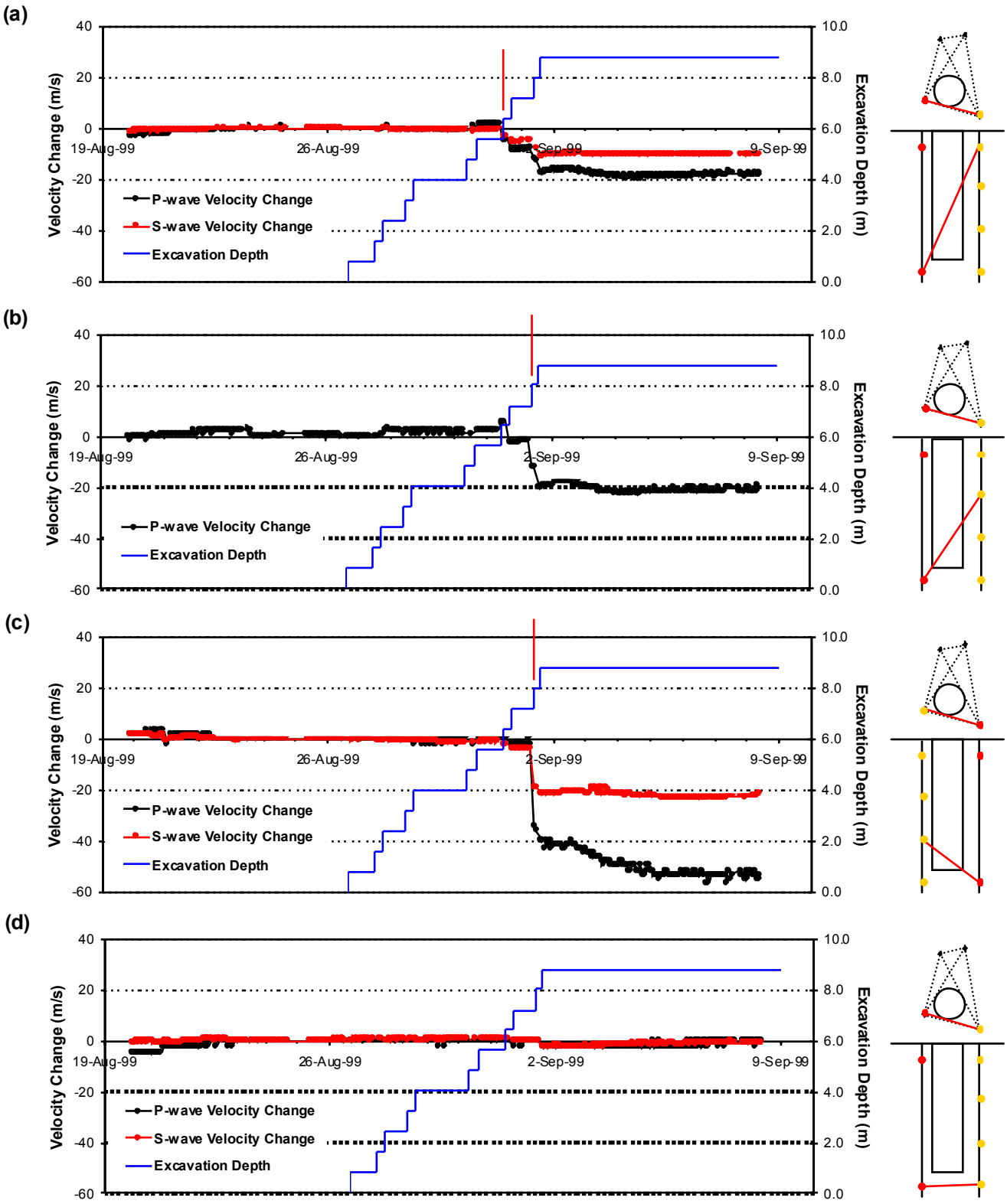

Figure 5-13: Velocity changes measured on ray path category 'S3' (Figure 5-11) for deposition hole DA3551G01. Ray paths shown are from a bottom transmitter to receivers with increasing depth: **a)** transmitter, t_n=4, receiver, r_n=1; **b)** t_n=4, r_n=2; **c)** t_n=2, r_n=7; **d)** t_n=4, r_n=4. Schematic diagrams in the right margin indicate the relative locations of transmitter (red) and receiver (gold). The red arrow indicates the passing depth defined in Figure 3-3.

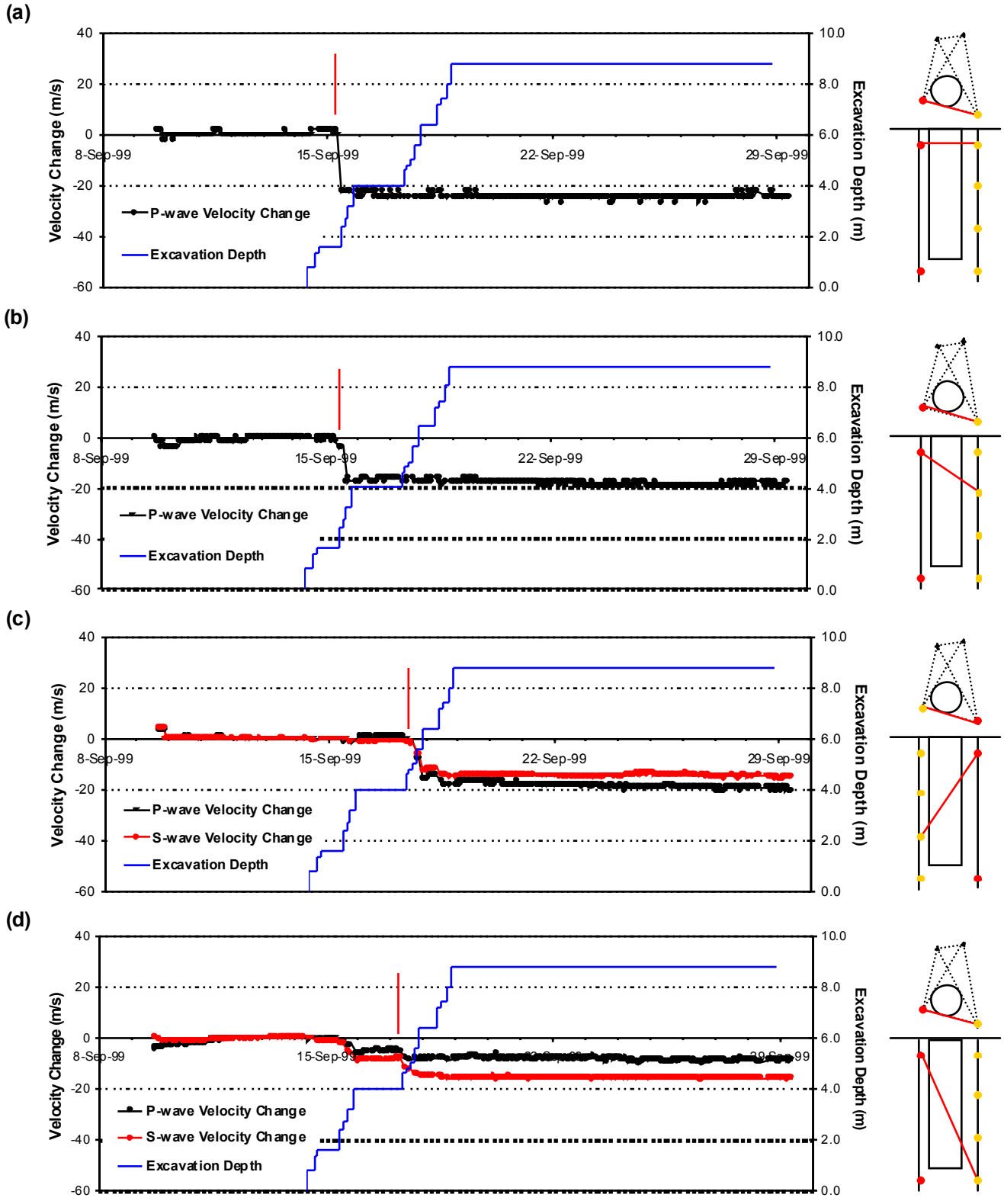

Figure 5-14: Velocity changes measured on ray path category 'S3' (Figure 5-11) for deposition hole DA3545G01. Ray paths shown are from a top transmitter to receivers with increasing depth: **a)** transmitter, t_n=3, receiver, r_n=1; **b)** t_n=3, r_n=2; **c)** t_n=1, r_n=7; **d)** t_n=3, r_n=4. Schematic diagrams in the right margin indicate the relative locations of transmitter (red) and receiver (gold). The red arrow indicates the passing depth defined in Figure 3-3.

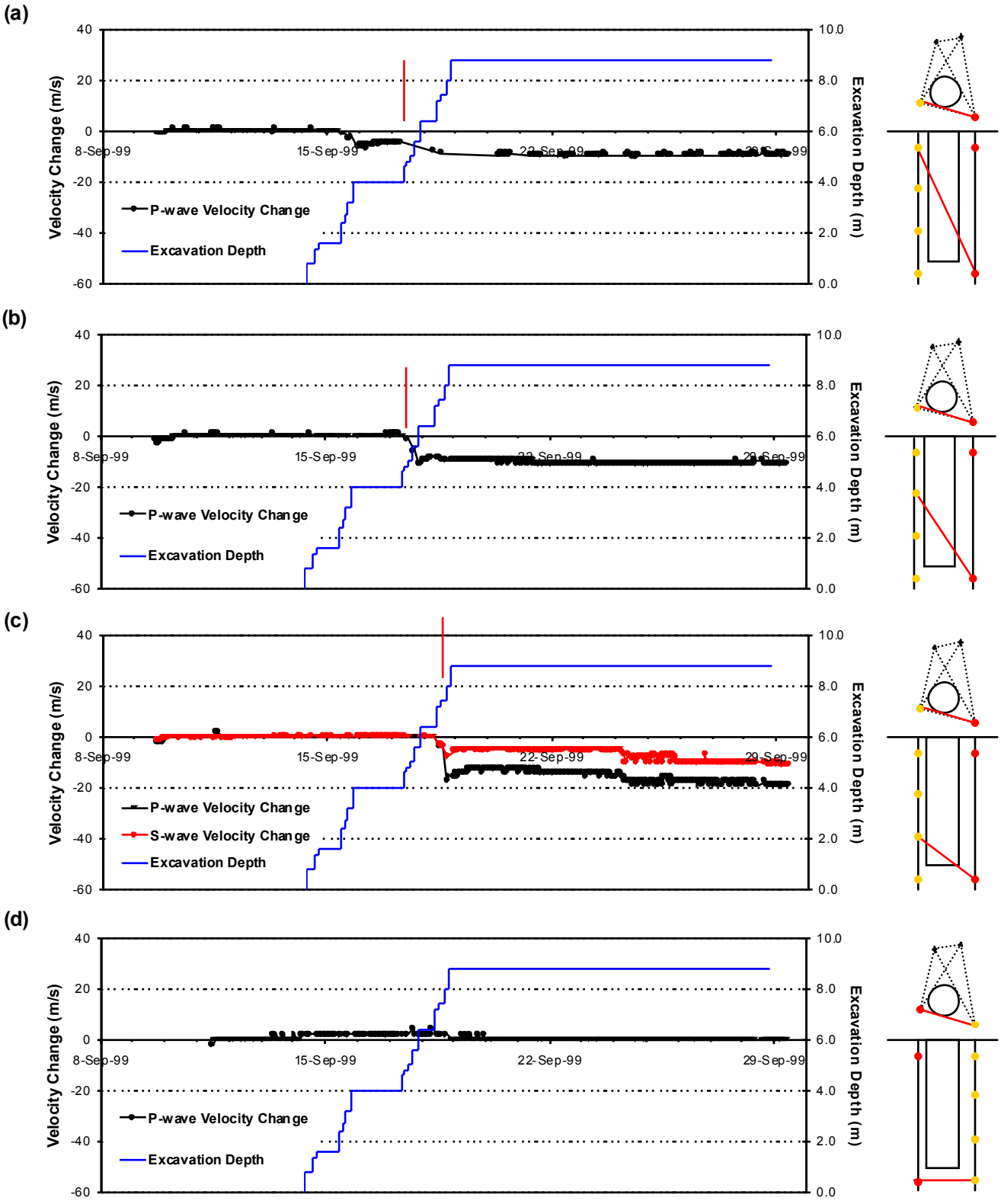

Figure 5-15: Velocity changes measured on ray path category 'S3' (Figure 5-11) for deposition hole DA3545G01. Ray paths shown are from a bottom transmitter to receivers with increasing depth: **a)** transmitter, t_n=2, receiver, r_n=5; **b)** t_n=2, r_n=6; **c)** t_n=2, r_n=7; **d)** t_n=4, r_n=4. Schematic diagrams in the right margin indicate the relative locations of transmitter (red) and receiver (gold). The red arrow indicates the passing depth defined in ***Figure 3-3***.

Figure 5-17 shows the ray path categories from the Prototype Tunnel superimposed onto the velocity model. It should be noted that because of the length and orientations of the ray paths each one may pass through regions of different damage and stress disturbance. Opening cracks caused by stress release or damage act to decrease the velocity causing a negative velocity change. Closing cracks caused by increases in compressive stress produce positive velocity changes. These effects are well documented in the laboratory (e.g. *King et al.*[1997]).

As can be seen from *Figure 5*-16 and *Figure 5*-17 the ray path category S1 passes through a region of damage associated with located AEs. The increased damage will act to decrease the observed velocity. However, the ray path also travels through a region of high compressive stress (from a simple Kirsch solution) that will act to increase the velocity. These effects result in a small net change. In comparison ray path categories S2 and S3 pass through regions of stress release and tensile damage - if the stress ratio is sufficient (K>3). The result is a large negative velocity change. The other three categories travel through regions of small stress disturbance and hence are only effected to a minor extent. *Maxwell and Young*[1995] mapped a similar velocity field around the Mine-by Tunnel at the Underground Research Laboratory (URL), Canada.

The mean velocity change for the skimming ray paths is -14.8m.s^{-1} for deposition hole DA3551G01 and -14.3m.s^{-1} for DA3545G01. This is again in agreement with that observed in the Retrieval Tunnel. If it is assumed that this average decrease is caused by fracturing in the damaged zone then using the method described in *ASC*[1999a] this results in a 15% decrease in dynamic Young's modulus in this region.

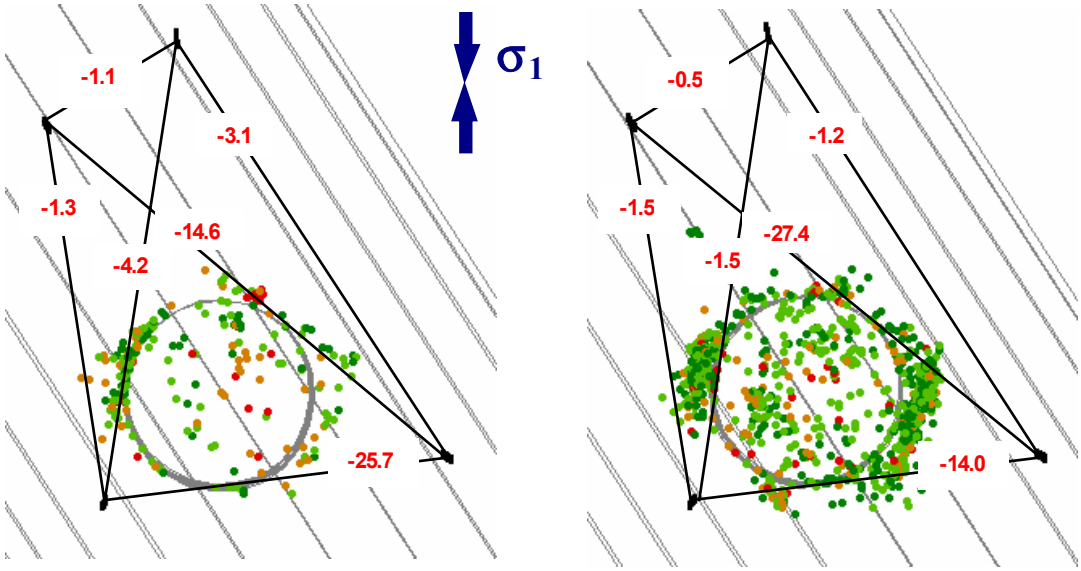

Figure 5-16: Plan views of the two deposition holes with located AEs: Left - DA3551G01; Right - DA3545G01. The views have been rotated so that σ_1 is up the page. Superimposed onto the plots are the six ray path categories of Figure 5- with mean velocity changes indicated.

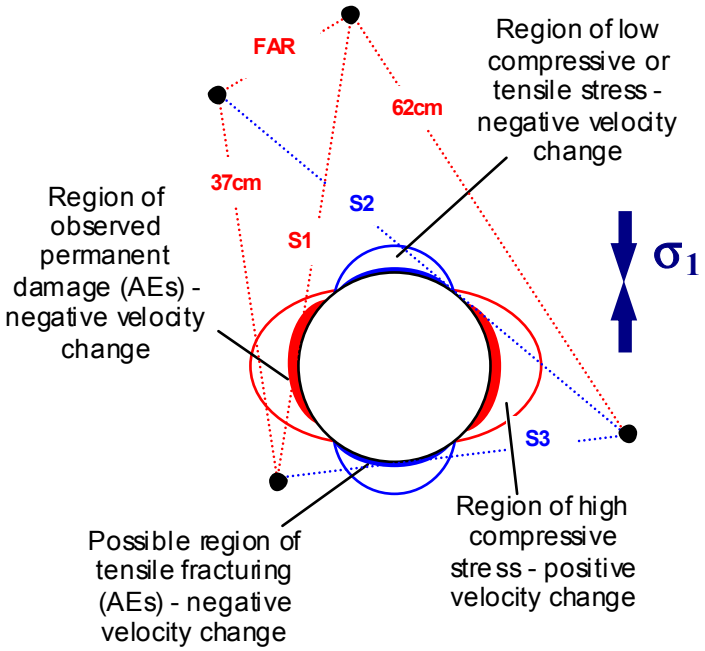

Figure 5-17: Interpretation of the ultrasonic results in terms of disturbed and damaged regions around the deposition hole. Regions of high stress anomalies are shown as expected from a Kirsch solution and the σ_1 orientation. Also indicated are regions of permanent damage associated with observed AE clustering. Ray paths observed with relatively high velocity decrease are shown in blue.

6 Results Summary and Conclusions

1. Ultrasonic velocities have been measured prior to the excavation of each deposition hole. Mean P-wave velocities of 5988 and 6013 $m.s^{-1}$ have been calculated for deposition hole DA3551G01 and DA3545G01respectively. Mean S-wave velocities are respectively 3392 and 3397 $m.s^{-1}$. The rock mass has been shown to be isotropic in both cases. These results differ from those observed in the Retrieval Tunnel where a 3% anisotropy was observed and mean velocities were approximately 80 $m.s^{-1}$ lower. The difference is probably due to a slight change in rock type being experienced at the 450m level to that at the 420m level. This change may be associated with different mineral, or pre-existing microfracture, alignment.

2. Stress measurements performed in the Prototype Tunnel [*Ljunggren and Bergsten*, 1998] are inconsistent with other measurements performed throughout the HRL [*Leijon*, 1995]. *Young et al.*[1996] use an average stress tensor (*Table 4-1*) calculated from the results presented by *Leijon*[1995]. Acoustic emission (AE) locations and velocity changes observed in the Retrieval Tunnel were consistent with the orientation of σ_1 given by this tensor [*ASC*, 1999a]. The stress tensor measured by *Ljunggren and Bergsten*[1998] has approximately the same principal stress magnitudes as the average stress tensor from *Leijon*[1995], however it is rotated by approximately 45^o azimuth and 45^o plunge. Results of AE locations from the deposition holes in the Prototype Tunnel are consistent with the orientation of the average stress tensor from *Leijon*[1995] and not with that obtained by *Ljunggren and Bergsten*[1998] in the Prototype Tunnel. Changes in velocity observed during excavation are also consistent with this stress tensor.

3. Velocity changes have been measured with a resolution of $\pm 2 m.s^{-1}$. A sharp decrease in velocity of between -10 to -30 $m.s^{-1}$ is observed on 'skimming' ray paths that pass within a few centimetres of the excavation. These changes occur over 1-3 rounds as the excavation of the deposition hole passes the ray path. The largest changes are observed for ray paths that pass through a region of low compressive or tensile stress given parallel to σ_1 in a simple Kirsch solution. The change is then associated with microcrack damage in this region accumulated over a few rounds of excavation. These microfractures are opened by the unloading of the compressive stress and result in a large decrease in measured velocity. In comparison, skimming ray paths that pass through the compressive stress region of the deposition hole do not show such large changes in velocity. The stress regime acts to close fractures in this region. A mean change of approximately -15 $m.s^{-1}$ is observed from all the skimming ray paths. An identical result was observed in the Retrieval Tunnel. Such a change yields an estimated decrease of 15% in the dynamic Young's modulus of the damaged zone around the deposition hole [*ASC*, 1999a].

4. A total of 2467 AE triggers were recorded during excavation of the two deposition holes in the Prototype Tunnel. Of these 1153 have produced AE locations. Calibration tests performed in the excavated deposition holes yield an estimated maximum uncertainty of 10cm in any AE location. Pencil lead breaks have been recorded from the interior of each deposition hole showing that the ultrasonic arrays are sensitive enough to pick up cracking on the millimetre scale; approximately the grain size of the rock. Sensitivity differences between the ultrasonic arrays, acquisition system and processing techniques for each of the deposition holes has been shown to be negligible. However,

of the total AE triggers only 16% occurred during excavation of deposition hole DA3551G01. Large differences in trigger rates were observed between the two holes with rates in DA3551G01 never reaching >30 events per hour. Rates in DA3545G01 reached a maximum of >150 events per hour. These differences could be explained by any, or a combination, of: a) macroscopic fractures being more prevalent in DA3545G01; b) excavation of DA3551G01 disturbing the stress field in the volume of DA3545G01; c) differences in excavation method.

5. AE locations show a clustering of events, and hence intense fracturing, occurring in regions orthogonal to the maximum principal stress, σ_1. This is in regions of high compressive stress given by a simple Kirsch solution and hence where breakout fracturing would be predicted. It must be noted that the scale of fracturing is probably of the order of millimetres and hence may not be discernible by eye. Microscope or dye impregnation tests may confirm these results. Such breakout fracturing was modelled in the Prototype Tunnel by [*ASC*, 1999b]. Furthermore, induced damage is not continuous down the deposition hole length but instead locates in distinct clusters. These are probably associated with pre-existing weaknesses in the rock mass such as macroscopic fractures. AE locations show these features to be more extensive in deposition hole DA3545G01 than in DA3551G01. The most notable clusters occur at depths associated with round 3 in DA3551G01 and with rounds 4-5 and 8-10 in DA3545G01. The furthest extent of the damaged zone represented by these clusters is 20-30cm into the rock wall. As well as breakout fracturing, AEs are also observed in regions parallel to σ_1 although in clusters much smaller in dimension (10s of centimetres). These may be associated with low compressive stresses, or tensile stresses, causing pre-existing fractures to open. A small AE cluster is observed approximately 80cm into the rock mass from the sidewall of DA3545G01, during excavation of round 10. This may be due to induced stresses causing disturbance on a pre-existing fracture.

7 Recommendations

The following observations can be summarised from the results of this report and from a similar study performed in the Canister Retrieval Tunnel.

a) There is a link between induced damage around a deposition hole (microcracking) and the intersection of excavation with pre-existing fractures. The variability in the location, extent and number of AE clusters around each deposition hole is probably mainly dependent on the number and orientation of these fractures. Fractures intersecting the excavation act as weaknesses that induce extensive damage in localised regions.

b) AE distributions and velocity measurements can give insights into the *in situ* stress orientation. 'Breakout' fracturing is observed in regions of high compressive stress orientated orthogonal to σ_1. Velocity measurements show relatively large decreases through regions associated with compressive stress unloading or tension. The orientations of principal stresses are consistent with the average *in situ* stress tensor for the HRL calculated from *Leijon*[1995]. However, they are not consistent with the orientations of *in situ* stresses in the Prototype Repository Tunnel measured by *Ljunggren and Bergsten*[1998].

It is therefore recommended that the following studies be performed to investigate these relationships. These studies are split into three components.

Component 1: Examining the stress field using AEs.

- **Back calculation of principal stresses.** Source mechanisms should be produced for AEs where possible [*Pettitt*, 1998]. The stress field can then be back calculated from AE locations using inversion of the source mechanism data. The volume of AE data should allow a constrained and cost effective method. The resulting stress field should then be compared to stress measurements already performed at the HRL to test inconsistencies in the measurements.

- **Failure criteria for AEs.** Failure stresses should be computed at all AE source locations using an elastic-modelling package. This will produce stress criteria for the observed microcracking. These can then be related to criteria established through existing laboratory data to understand the effect of fractures on locally weakening the rock mass.

- **Effect of stress transfer.** The effect of stress transfer between deposition holes should be investigated by repeating the above with or without neighbouring deposition holes. Does one deposition hole effect the stress regime experienced by a neighbour sufficiently to induce greater AEs on existing fractures?

Component 2: The structure of rock damage.

- **Relationship between AE clusters and mapped fracture intersections/orientations.** Deposition hole maps should be correlated with AE cluster locations. Do only certain kinds of fractures, or those with particular orientations, have an effect on the AE?

- **Using AE mechanics to investigate fracture pathways through the damaged zone.** The source mechanics allow an interpretation of the failure mode and orientation. The mechanisms and locations of AEs can then be related to fracture orientations and can be used to map potential fracture pathways through the damaged zone.

- **Crack density and saturation.** The P- and S-wave changes measured through the damaged zone should be inverted for crack density and saturation. Ray paths passing through different regions of the deposition hole wall could then be used to construct a crack density model around the deposition hole.

Component 3: AEs and geomechanical models.

- **Sensitivity of models to principal stresses.** Modelling of the rock response has been a key component to the design and construction of the Prototype Repository. The modelling of e.g. ASC[1999b] should be repeated with different principal stresses in order to get a feel for the sensitivity of these models to the principal stress field.

- **Analysis of the dependence of AEs on fractures in numerical models.** A follow-up study to *ASC*[1999b] should be performed using a fracture network built into the Particle Flow Code (PFC) models. Is there a relationship between microcracking (AEs) generated in the models and this fracture network? If so, can the results of this modelling be related to those observed *in situ*?

8 References

ASC, *Acoustic Emission and Ultrasonic Monitoring During the Excavation of Deposition Holes in the Canister Retrieval Test*, SKB/Äspö 03, Applied Seismology Consultants Ltd, Shrewsbury, UK, 1999a.

ASC, *A Three Dimensional Discontinuum Model of the Excavation of a Deposition Hole at the Äspö HRL*, SKB/Äspö 04, Applied Seismology Consultants Ltd, Shrewsbury, UK, 1999b.

ASC, *Ultrasonic Monitoring During the Excavation of Deposition Boreholes in the Prototype Tunnel: Trip Report and Data Description*, SKB/Äspö 05, Applied Seismology Consultants Ltd, Shrewsbury, UK, 1999c.

Breckenridge, F.R., T.M. Proctor, N.N. Hsu, S.E. Fich, and D.G. Eitzen, Transient sources for acoustic emission work, in *Proc. 10th Int. Acoust. Emission Symp., NDI Japan*, pp. 20-37, 1990.

Falls, S.D., and R.P. Young, Examination of the excavation disturbed zone in the Swedish ZEDEX tunnel using acoustic emission and ultrasonic velocity measurements, in *Proceedings of Eurock '96, Turin, Italy, 1996*, Balkema, Rotterdam, pp. 1337-1344, 1996.

Falls, S.D., and R.P. Young, Acoustic emission and ultrasonic-velocity methods used to characterise the excavation disturbance associated with deep tunnels in hard rock, *Tectonophysics*, *289*, 1-15, 1998.

Gibowicz, S.J., and A. Kijko, *An Introduction to Mining Seismology*, Academic Press, 1994.

King, M.S., A. Shakeel, and N.A. Chaudhrey, Acoustic wave propagation and permeability in sandstones with systems of aligned cracks, in *Developments in Petrophysics*, edited by M.A. Lovell, and P.K. Harvey, Geological Society Special Publication No. 122, pp. 69-85, 1997.

Leijon, B., *Summary of Rock Stress Data from Äspö*, Äspö Hard Rock Laboratory Progress Report 25-95-15, Swedish Nuclear Fuel and Waste Management Company, Sweden, 1995.

Ljunggren, C., and K.-Å. Bergsten, *Rock Stress Measurements in KA3579G*, Äspö Hard Rock Laboratory Progress Report HRL-98-09, Swedish Nuclear Fuel and Waste Management Company, Sweden, 1998.

Ljunggren, C., and H. Klasson, *Rock Stress measurements at the ZEDEX test area, Äspö HRL*, Äspö Hard Rock Laboratory Technical Note TN-96-08z, Swedish Nuclear Fuel and Waste Management Company, Sweden, 1996.

Martin, C., and N. Chandler, Stress heterogeneity and geological structures, *Int. J. Rock Mech. Min. Sci. and Geomech. Abstr.*, *30*, 993-999, 1993.

Maxwell, S.C., and R.P. Young, A controlled in-situ investigation of the relationship between stress, velocity and induced seismicity, *Geophys. Res. Lett.*, *22*, 1049-1052, 1995.

Patel, S., L.-O. Dahlstrom, and L. Stenberg, *Characterisation of the Rock Mass in the Prototype Repository at Äspö HRL Stage 1*, Äspö Hard Rock Laboratory Progress Report HRL-97-24, Swedish Nuclear Fuel and Waste Management Company, Sweden, 1997.

Pettitt, W.S., *Acoustic emission source studies of microcracking in rock*, Ph.D. thesis, Keele University, Keele, Staffordshire, UK, 1998.

SKB, *Äspö Hard Rock Laboratory: Current Research Projects 1998*, Swedish Nuclear Fuel and Waste Management Company, Sweden, 1999.

Urbancic, T.I., C.-I. Trifu, and R.P. Young, Microseismicity derived fault-planes and their relationship to focal mechanism, stress inversion, and geologic data, *Geophys. Res. Lett.*, *20* (22), 2475-2478, 1993.

Young, R.P., C.D. Martin, R. Murdie, J. Alcott, S. Falls, I. Stimpson, and S. Yazici, *Numerical Modelling, Acoustic Emission and Velocity Studies of the Excavation Disturbed Zone at the Hard Rock Laboratory*, Äspö Hard Rock Laboratory Technical Note, Swedish Nuclear Fuel and Waste Management Company, Sweden, 1996.

Zeng, L., and L.-O. Dahlström, *Prototype Repository: Finite Element Analyses of Mechanical Consequences due to the Rock Excavation and Thermal Load*, Äspö Hard Rock Laboratory Technical Note, Swedish Nuclear Fuel and Waste Management Company, Sweden, 1999.

9 Appendix

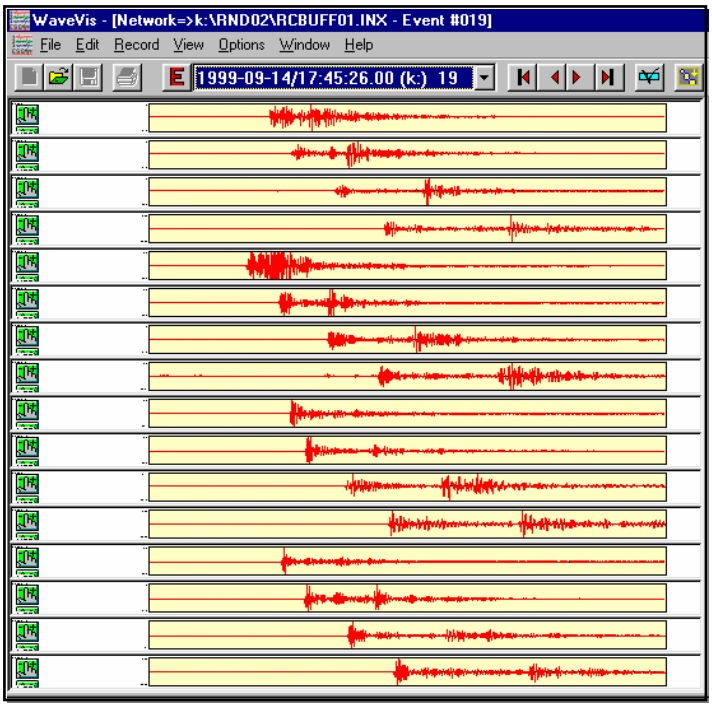

Figure A1: *Waveforms from an AE recorded shortly after cessation of drilling of deposition hole DA3545G01 at 1.63m depth (Round #2).*

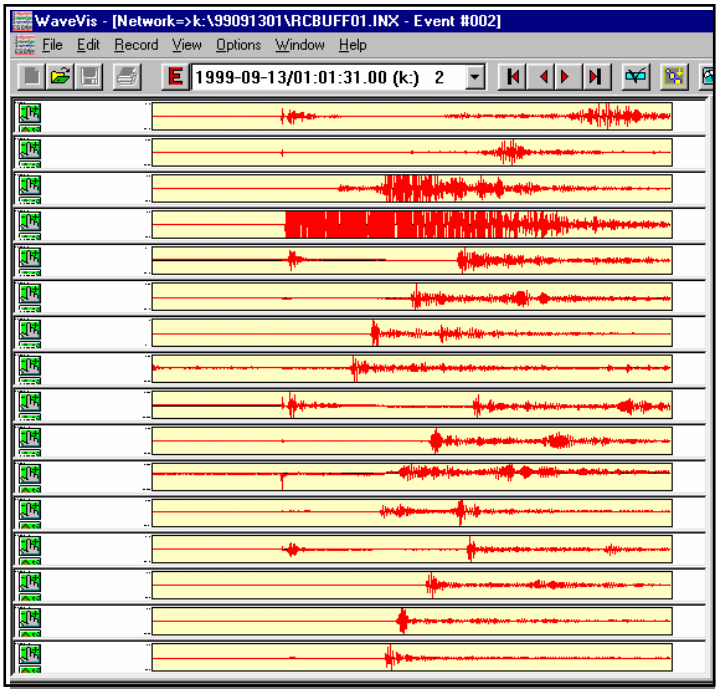

Figure A2: *Example waveforms from a ultrasonic survey 99091301 conducted immediately before the start of excavation of deposition hole DA3545G01.*

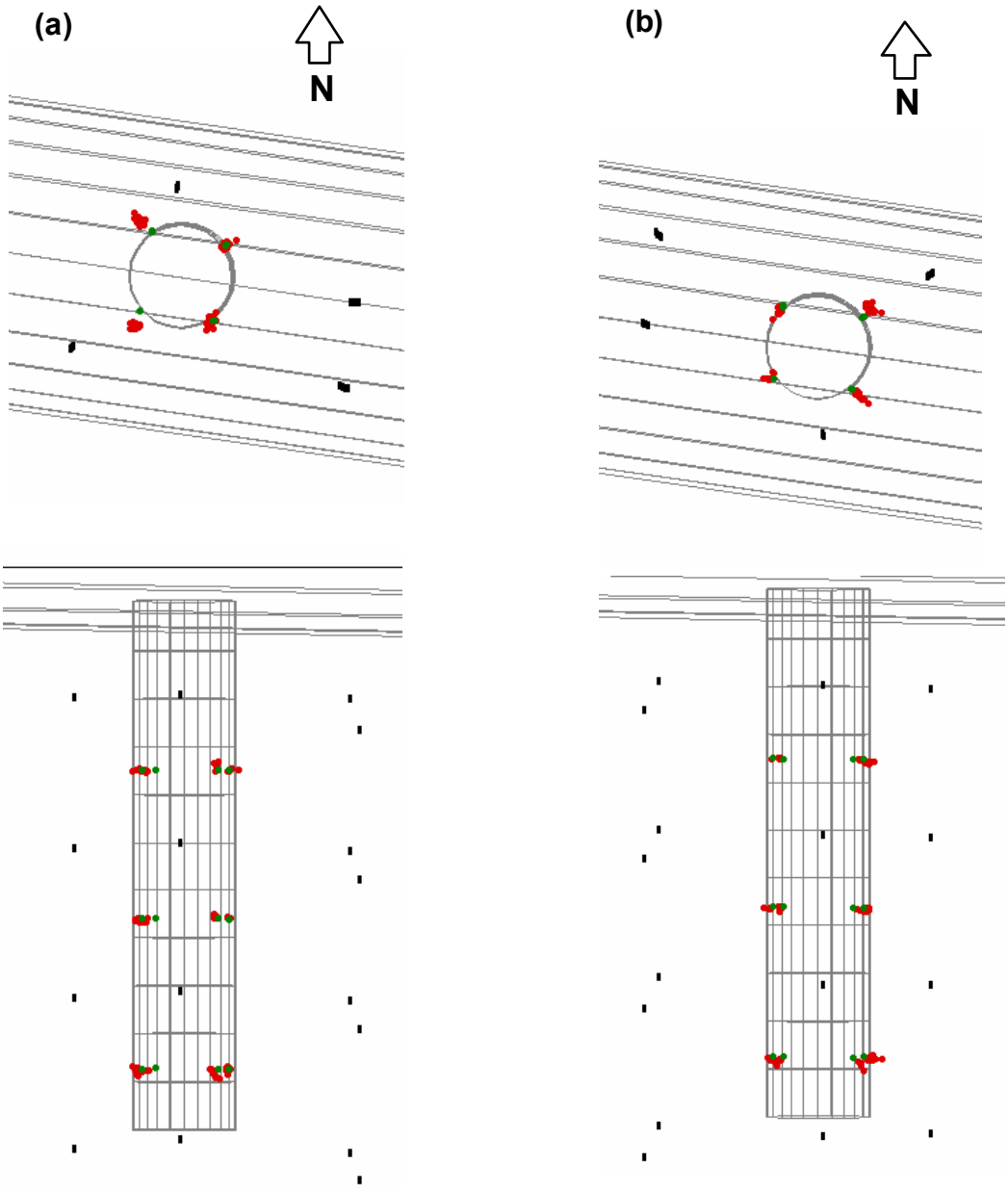

Figure A3: *Computed locations for Schmiddt shots (red markers) conducted in a) DA3551G01 and b) DA3545G01. Upper plots are in plan and lower plots in cross-section. Green markers are the true shot locations calculated from survey points on the tunnel floor. Black markers are receiver locations.*

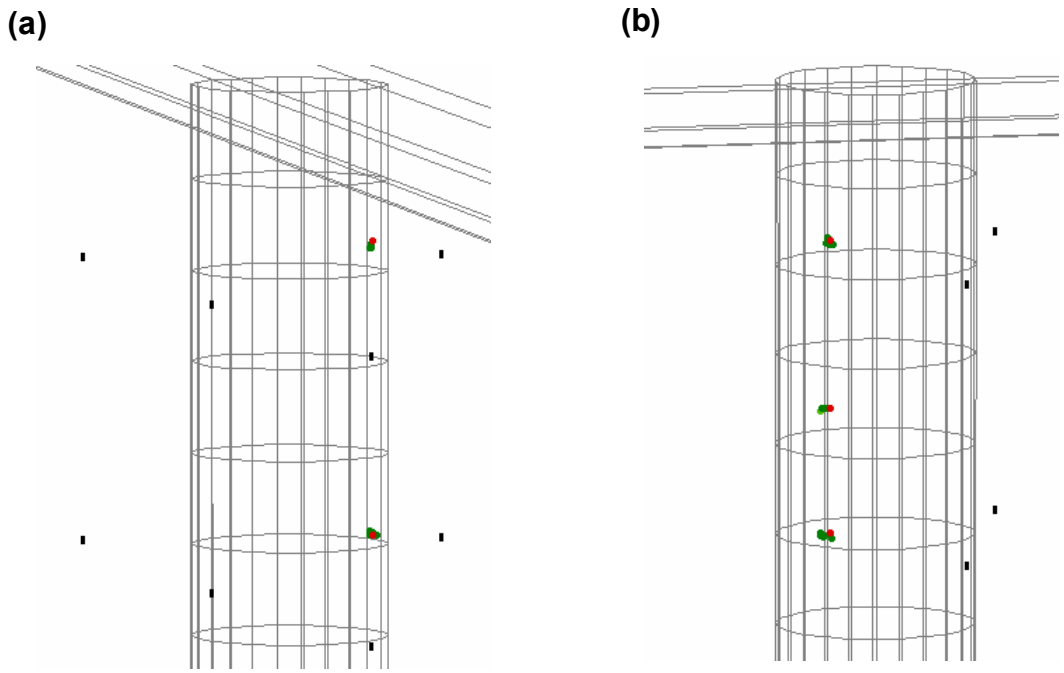

Figure A4: *Computed locations of pencil break tests (green markers) conducted in a) DA3551G01 and b) DA3545G01. Red markers are true locations calculated from survey points on the tunnel floor.*

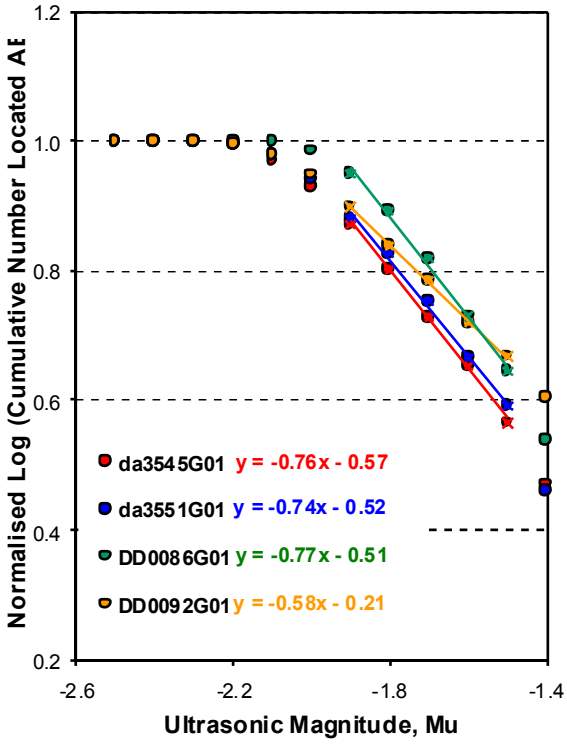

Figure A5: *Relationship of number of AEs located for the four monitored deposition holes (*Table 5-1*) with magnitude. The figure shows a 'b-value' plot (e.g.* Gibowicz and Kijko *[1994]) for each deposition hole. Each plot is normalised to 1.0 so that they fit on the same vertical scale. According to seismic theory the graph is linear across the range of magnitudes where the complete event data set is monitored by the array. The b-value is the slope of the graph across this range.*